OPERATING PEROVSKITE SOLAR CELL UNDER CONCENTRATED SOLAR LIGHT

by

Yen Jung Tu

B.S, National Cheng Kung University, 2013

Submitted to the Graduate Faculty of

Swanson School of Engineering in partial fulfillment

of the requirements for the degree of

Master of Science

University of Pittsburgh

2016

UNIVERSITY OF PITTSBURGH

SWANSON SCHOOL OF ENGINEERING

This thesis was presented

by

Yen Jung Tu

It was defended on

March 28th, 2016

and approved by

Jung-Kun Lee, PhD, Associate Professor

Department of Mechanical Engineering and Materials Science

Qing-Ming Wang, PhD, Professor

Department of Mechanical Engineering and Materials Science

Smolinski Patrick, PhD, Associate Professor

Department of Mechanical Engineering and Materials Science

Thesis Advisor: Jung-Kun Lee, PhD, Associate Professor

OPERATING PEROVSKITE SOLAR CELL UNDER CONCENTRATED SOLAR LIGHT

Yen Jung Tu, M.S.

University of Pittsburgh, 2016

A recent forecast suggested that solar cell industry will contribute nearly one third of new electricity generation capacity worldwide by the year 2030.[1] Silicon solar cell is the most widely used photovoltaic device nowadays. However, opportunities exist for technologies that advance either higher efficiencies or lower fabrication cost in the silicon solar cell. Thus, the emergence of organic–inorganic halide perovskite based solar cell has attracted much attention during the past few years. Compared with traditional silicon solar cell, the perovskite solar cell has a lower cost and is easy to fabricate. Additionally, the high potential is another feature that catches peoples' eyes. With the first perovskite solar cell reported in 2009 with power conversion efficiency of 3.8%. A record efficiency of 21.0% was achieved by researchers at EPFL in late 2015.[2] However, the instability of perovskite solar cell at high temperature reduces the performance. Modern solar cell design often uses lens to concentrate solar light in order to produce higher power from small area of solar cells. Nevertheless, part of the solar power will be converted into heat and increase the temperature of the cell. When it comes to perovskite solar cell, the concentrated solar light gives rise to considerable temperature increase of the glass substrate and causes significant degradation

of the perovskite layer. Thus, figuring out the performance of perovskite solar cell under evaluated temperature and the temperature raise according to different incident light intensity are important jobs for designing concentrator solar cells. In this thesis, the transmittance and reflectance were simulated by Lumerical FDTD software to calculate the absorbance of perovskite solar cell under different incident light intensity. The temperature evaluation was then calculated by Ansys Mechanical software to find out the relation between incident light power and temperature increase. To characterize the performance of perovskite solar cell under different temperature, the I-V curve and incident photon-to-current efficiency (IPCE) were measured under various temperature conditions. By comparing the temperature-light intensity correlation, IPCE performance and I-V curve, the suitable incident solar light intensity for operating perovskite solar cell was found.

TABLE OF CONTENTS

LIST OF TABLES

LIST OF FIGURES

NOMENCLATURE

PCE	Power conversion efficiency
IPCE	Incident photon-to-current efficiency
E_c	Conduction band
E_v	Valence band
E_g	Band Gap
EHP	Electron-hole pair
$\boldsymbol{\lambda}$	Wavelength
h	Planck's constant
c	Speed of light
HTM	Hole transporting material
I_{sc}	Short-circuit current
J_{sc}	Short-circuit current density
V_{oc}	Open-circuit voltage
FF	Fill factor
P_{in}	Incident solar light power
q	Electron charge
$F(\lambda)$	AM1.5G solar spectrum
$\boldsymbol{t}$	Tolerance factor
$\boldsymbol{\mu}$	octahedral factor
FTO	Fluorine doped tin oxide

ITO	Indium doped tin oxide
PSC	Perovskite solar cell
NP	Nanoparticle
NW	Nanowire
FDTD	Finite-difference-time-domain
%T	Transmittance
%R	Reflectance
%A	Absorbance
FEM	Finite element method
UV	Ultraviolet
IR	Infrared
DC	Direct current
AC	Alternate current
DSC	Dye-sensitized solar cell

ACKNOWLEDGMENT

First of all, I would like to give my sincere gratitude to my advisor, Prof. Jung-Kun Lee for his patience and considerable help, allowing me to take this project and make it successful. Without his guidance and support, I would have never completed this thesis.

I would also want to express my appreciation to my committee members, Prof. Qing-Ming Wang and Prof. Smolinski Patrick for their time and valuable feedback.

I would also like to thank my group members: Dr. Gill-Sang Han, Salim Caliskan and Ziye Xiong, Fangda Yu, Fen Qin and Seongha Lee for their experience and helpful discussion.

Last but not the least; I would have my thanks to my family for supports and encouragements.

1.0 BACKGROUND AND LITERATURE REVIEW

This chapter offers an introduction to semiconductor, P-N junction and solar cells. Some quantitative parameters such as I-V curve, Power Conversion Efficiency (PCE) and Incident photon-to-current efficiency (IPCE) are presented. The main topic of this thesis, perovskite solar cell, will also be introduced. The basic concepts of Finite Element Method and Finite Difference Time Domain method are covered in order to have a better understanding of Ansys and Lumerical FDTD software.

1.1 SEMICONDUCTOR AND PHOTONS

Semiconductors are crystalline or amorphous solids with distinct electrical characteristics.[3] The structure of semiconductor is built up by covalent bonds. Group IV atoms such as silicon are the most commonly used materials since they have 4 valence electrons. When forming covalent bonds, the 4 valence electrons are shared by surrounding atoms to form a stable structure.

The electric conductivity behavior of semiconductor is between conductors and insulators. One significant difference between conductor and semiconductor is their band structure. For conductors such as metals, electron energy levels are continuously distributed. However, a band gap exists between conduction band (Ec) and valence band (Ev) in semiconductor.[4] Normally, electrons in semiconductors stay in valence band and this is considered a stable bond structure.

The minimum energy required to excite an electron from valence band to conduction band is called the band gap (E_G). When a semiconductor is exposed to thermal energy or a photon containing energy larger than the band gap, the electron on the valence band can jump to the conduction band and leave a hole with positive charge in its previous location. The process of electrons jumping from Ev to Ec is called electron excitation. This electron and hole are called electron-hole pair (EHP) and can move freely, which makes the semiconductor conductive. The electrons and holes are also called carriers. The sketch of electron excitation is shown in figure 1.1.

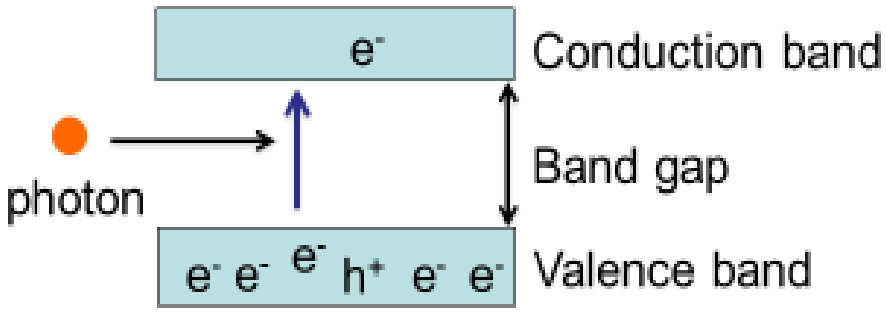

Figure 1.1 Sketch of electron excitation

Doping is a common technique to adjust the balance of electrons and holes in a semiconductor. The result of doping can be classified into "n-type" and "p-type" semiconductors. Group V atom, having 5 valence electrons, is doped into group IV atoms to produce n-type semiconductors. Since only 4 valence electrons from each atom are used to form covalent bond, the one extra electron is free to move and can participate in conduction. On the other hand, doping group III atoms into group IV atoms can produce p-type semiconductors with extra holes. Because group III atom only has 3 valence electrons, this results in a hole that can move freely. In the above cases, group V atoms are called n-type dopant and group III atoms are called p-type dopant.

Photons are seen as the basic component of light. Photons can display both properties of waves and particles and this feature is called “wave-particle duality”. Each color of light consists of distinct photons with different energy and wavelength. The relationship of energy contained in a photon and the wavelength can be expressed as:

$$E = \frac{hc}{\lambda} \tag{1.1}$$

Where E is the energy contained in a photon, λ is the wavelength, h is Planck's constant and c is the speed of light. Thus, a photon can be characterized either by energy or wavelength. As the wavelength of a photon gets longer, the energy contained decreases.

1.2 P-N JUNCTION AND SOLAR CELL

1.2.1 P-N Junction

P-N junctions are formed by joining n-type and p-type semiconductor materials.[5] In the P-N junctions, electrons near the interface diffuse from n-type to p-type since the n-type has a higher concentration of electrons, leaving behind positive charges in the n-type. On the other hand, holes near the interface flow from p-type to n-type and leave negative charges in the p-type. Thus, the interface region would lose its neutrality and start to form a space charge region, which builds up an electric field that prevent the diffusion process for both electrons and holes. In the P-N junction, there are two phenomena happening at the same time, one is the diffusion process which tend to form more space charge region while the electric field built up by the space charge region try to hold in the diffusion. These two effects continues until equilibrium is established as shown in figure 1.2.

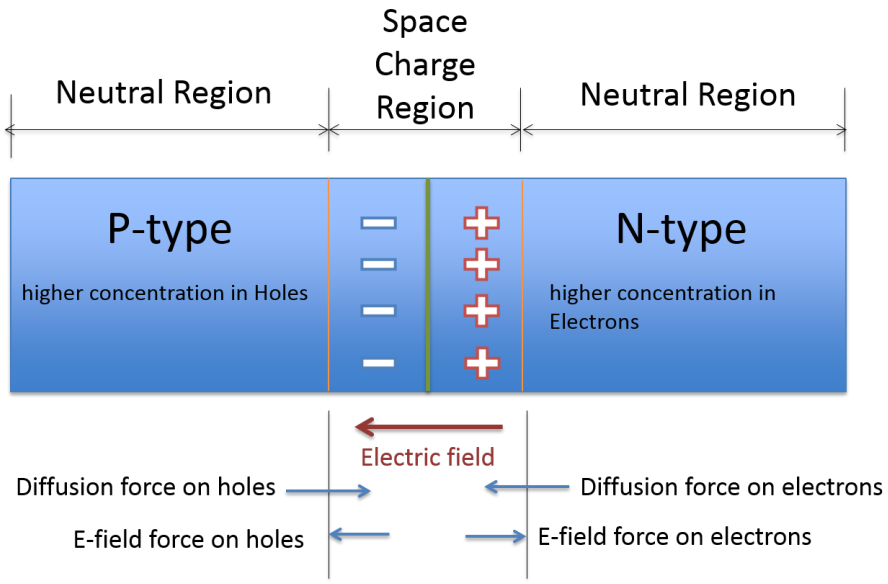

Figure 1.2 P-N junction equilibrium

1.2.2 Space Charge Polarization

Space charge polarization occurs when there is an accumulation of charge at an interface between two materials or between two regions within a material because of an external electric field.[6] Thus, the carriers will amass at the boundary and the material becomes polarized as shown in figure 1.3.

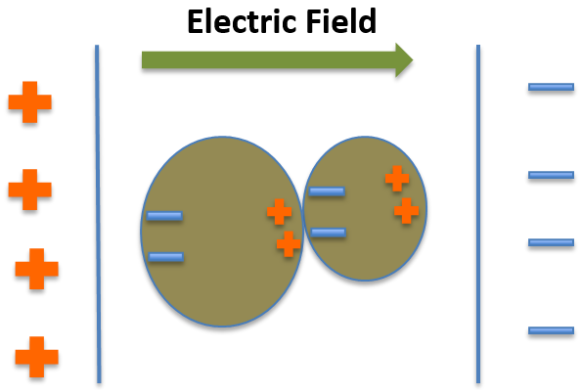

Figure 1.3 Plot for space charge polarization

This behavior is common in multiphase materials. Since the carrier transportation ability is limited, so this behavior response to alternative current (AC) when the frequency is less than 10^4Hz.[7] In P-N junction type solar cell such as perovskite solar cell, there is an electric field formed between the n-type layer and p-type layer. The light absorber layer is positioned in between of these two layers. Thus, this phenomenon would affect the operation of cell if the light absorber material is a multiphase material.

1.2.3 Solar Cell

A solar cell is a device that converts solar light energy into electric energy by photovoltaic effect. Normally, solar cells are made by P-N junctions. The operation of a P-N junction type solar cell requires firstly, the absorption of solar light. To produce light-generated current or photocurrent, the incident photon must contain energy higher than the band gap of the material in order to excite the electron from valence band to conduction band. Meanwhile, a hole with positive charge is left at where the excited electron previously stayed. As a result, the absorption of incident photon by the semiconductor material generates a free electron-hole pair. Second, the electron-hole pair is separated by the electric field built up by the p-n junction. In this manner, electrons move to the n-type side and holes move to the p-type side. If connected to an external circuit, the carriers can flow through the circuit and produce a current. For perovskite solar cell, the n-type material is called hole-blocking layer while the p-type material is call hole-transporting material (HTM).

1.2.4 I-V Curve

I-V curve (as shown in figure 1.4) is an important graph for determining the properties of a solar cell. There are three key characteristics contained in the I-V curve, the short-circuit current density (J_{sc}), open-circuit voltage (V_{oc}) and fill factor (FF). While the short-circuit current (I_{sc}) is defined as the current through a solar cell when the voltage is zero, the J_{sc} is the I_{sc} per unit area in order to eliminate the effect of solar cell area. On the other hand, when the current is equal to zero, the voltage at this point is called V_{oc}, which is the maximum voltage that can be generated by the cell under specific light exposure. However, the power output of cell is equal to zero under both J_{sc} and V_{oc} condition.

The FF, defined as the maximum power over the product of J_{sc} and V_{oc}, is an important parameter for investigating the power output of a solar cell and is considerably sensitive to solar cell's quality. For instance, series resistance, caused by the attaching defects at the interface between different layers in a solar cell, can conspicuously decrease the FF and lower the performance of solar cells. While at maximum power, there is a pair of corresponding voltage (denoted as V_m) and current (denoted as I_m). And the P_{max} is equal to $V_m * I_m$. Thus the FF can be expressed as below:

$$FF = \frac{V_m * I_m}{V_{oc} * I_{sc}} \tag{1.2}$$

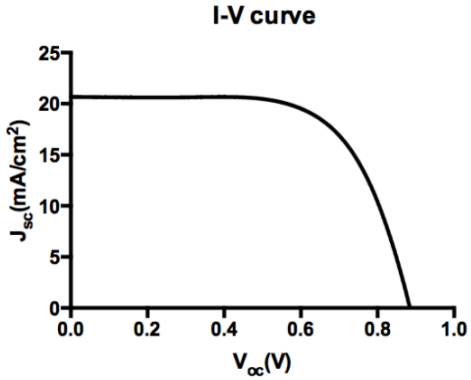

Figure 1.4 Common I-V curve

1.2.5 Power Conversion Efficiency

The power conversion efficiency (PCE), also called the efficiency, is the most common parameter to compare the performance between solar cells. It is defined as the electric energy generated by the solar cell over the input solar energy. In order to only study the performance of solar cell itself, the effects of spectrum and intensity of incident solar light need to be eliminated. Thus, the efficiency is normally measured under a standard AM1.5G spectrum (1000W/m^2).

The output power of the solar cell is defined as:

$$P_{generated} = FF * V_{oc} * I_{sc} \tag{1.3}$$

Thus, the equation of the PCE of a solar cell can be given by:

$$PCE = \frac{P_{generated}}{P_{in}} = \frac{FF * V_{oc} * I_{sc}}{P_{in}} \tag{1.4}$$

Where FF is the fill factor, V_{oc} is the open-circuit voltage, I_{sc} is the short-circuit current and P_{in} is the incident solar light power.

1.2.6 Incident Photon-to-Current Efficiency (IPCE)

Incident photon-to-electron conversion efficiency (IPCE) is one of the most important indicators of solar cells. It can be used for understanding current generation, recombination, and diffusion mechanism in the cell.[9] It offers more information about a solar cell than I-V curve. IPCE is defined as the ratio of the number of carriers collected by the solar cell to the number of photons of incident light on the solar cell. It consists of a monochromator scanning different wavelength light in the spectral response range. The current generated by the solar cell is recorded as the wavelength of light changes continuously. Thus, IPCE is given as a function of the wavelength (λ), as shown in figure 1.5. Ideally, an incident photon with energy higher than the band gap results in a pair of excited EHP. In the real case, however, the number of EHPs reduces due to the recombination effect. Some of the EHPs recombine before they enter the external circuit. The formula of IPCE is expressed as the ratio of photon-generated electrons to the incident photons, as shown in Equation 1.5:

$$IPCE = \frac{1240 * I_{sc}}{\lambda * \frac{I_{photon}}{responsivity}} = \frac{1240}{\lambda(nm)} * \frac{I_{sc}(A)}{P_{incident\ photon}(W)} \qquad (1.5)$$

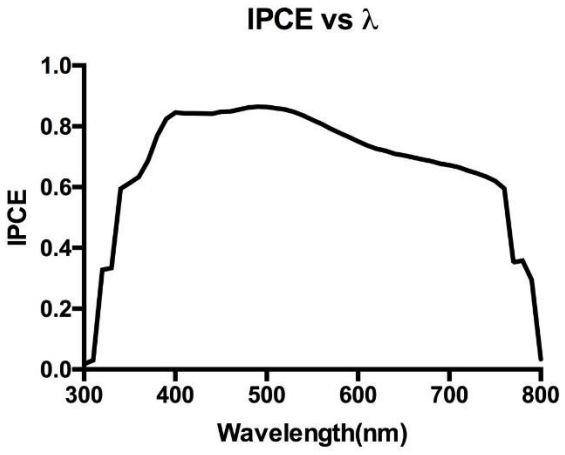

Figure 1.5 Graph of IPCE as a function of wavelength

By the definition of IPCE, the Jsc under AM 1.5G irradiation can be calculated by integrating the product of the incident monochromatic photon flux density (F (λ)) of AM 1.5 global solar spectrum and IPCE(λ) of the solar cell over the wavelength (λ) of the incident light.[9] The integration formula can be expressed as:

$$J_{sc} = q \int IPCE(\lambda) * F(\lambda)\, d\lambda \qquad (1.6)$$

Where q is the electron charge and F(λ) is the AM1.5G solar spectrum. The integration plot is shown as:

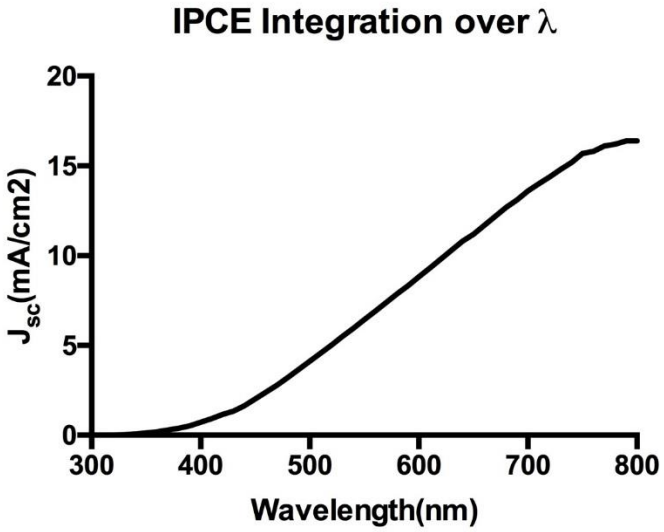

Figure 1.6 Plot of IPCE integration over wavelength

1.3 PEROVSKITE SOLAR CELL

1.3.1 Structure of Perovskite

Perovskites are materials described by the formula ABX_3, where X is an anion and A and B are cations of different sizes (A being larger than B). The crystal structure of perovskite is depicted in

figure 1.7[11], where A is positioned at (000) point, B is positioned at (½½½) and Xs are positioned at (½½0), (0½½) and (½0½). The formability and crystallographic stability of perovskite structure can be inferred by calculating the tolerance factor *t* and octahedral factor μ. Here, *t* is defined as the ratio of the distance between A-X to the distance between B-X in an idealized solid-sphere model ($t = (R_A + R_X)/\{\sqrt{2}(R_B + R_X)\}$, where R_A, R_B and R_X are the ionic radii of the corresponding ions) and μ is defined as the ratio R_B/R_X.[8][12] For the organic-inorganic halide perovskite commonly studied nowadays, the organic cation A is generally the methylammonium ($CH_3NH_3^+$) and cation B is Pb^{2+}. The halogen anion X is usually iodine (I^-), while Cl and Br are also investigated. The perovskite methylammonium lead triodide ($CH_3NH_3PbI_3$) is synthesized by PbI_2 reacting with methylammonium iodide (CH_3NH_3I) under room temperature. However, the stability of perovskite structure used in solar cell is usually limited. When exposed to moisture, air or other chemicals having active hydrogen atoms, the $CH_3NH_3PbI_3$ structure can break easily. This is followed by the decomposition of perovskite structure and causes a significant decrease in the efficiency.

1.3.2 Light Absorber Perovskite

The primary role of Perovskite ($CH_3NH_3PbI_3$) in Perovskite solar cell is to be the light absorber. The incident photons are absorbed by Perovskite and generate electron-hole pairs. Thus, it is the most crucial part in perovskite solar cells.

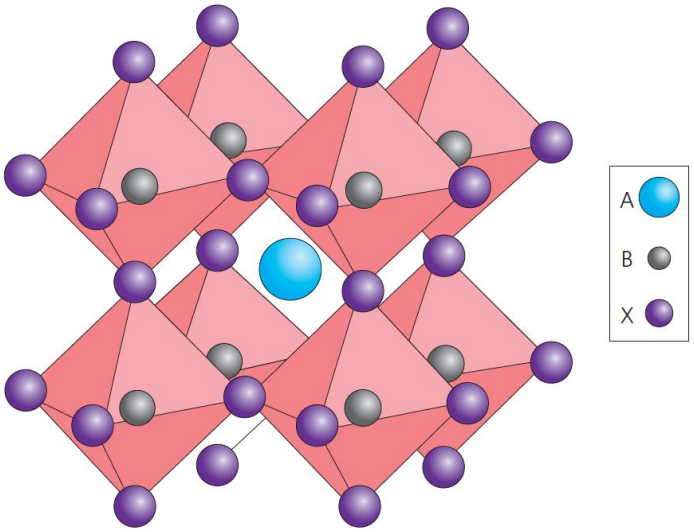

Figure 1.7 Perovskite Crystal Structure [8]

1.3.3 Synthesis Reaction

The synthesis of Perovskite ($CH_3NH_3PbI_3$) is the combination reaction of methylammonium iodide and lead iodide added together. As equation 1.7 shows:

$$CH_3NH_3I + PbI_2 \rightarrow CH_3NH_3PbI_3 \quad (1.7)$$

Currently two main synthesis methods are adopted mostly. The widely applied, simplest method is to dissolve CH_3NH_3I and PbI_2 together as precursor. The mixture is then spin-coated and annealed to form $CH_3NH_3PbI_3$ perovskite structure.[12][14] Another method is called Sequential deposition method or two step method,[15] in which the PbI_2 and CH_3NH_3I are prepared separately. First, the PbI_2 is deposited on the substrate by spin coating, and then it is dipped into CH_3NH_3I solution to synthesis Perovskite. The sequential method is generally believed to produce perovskite solar cell with better performance.

1.3.4 Perovskite Solar Cell Structure Types

The Perovskite solar cell, as a kind of thin film P-N junction solar cell, is an aggregation of light absorber perovskite, P-N junction, anode and cathode deposited on glass substrate. The anode plays a role on transporting electrons to external circuit. Indium doped tin oxide (ITO) and Fluorine doped tin oxide (FTO) are two commonly used materials for anode in perovskite solar cell. The n-type semiconductor, also called the hole blocking layer or electron transporting layer, is attached on the anode layer. Generally TiO_2 is used for n-type material. For the p-type semiconductor, Li^+ doped Spiro-OMeTAD is often utilized. While non-doped tetrathiafulvalene derivative (TTF-1) is proposed to be another potential p-type material offering high performance.[16] The cathode, linked to the p-type material, is commonly gold for its superior electrical conductivity and low resistivity. The main solar cell material, perovskite, is coated in between of the n-type and the p-type. Usually the mesoporous TiO_2 is firstly spin coated on the ITO or FTO glass substrate to transport electrons. Then the perovskite is deposited in the TiO_2 scaffold layer. TiO_2 is chosen as the scaffold layer because of its good conductivity and high transparency.

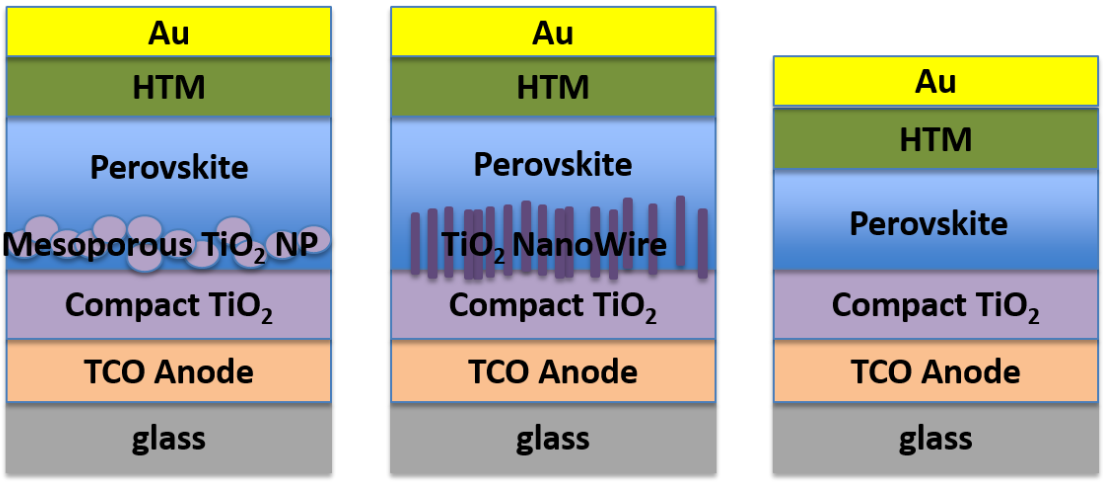

Figure 1.8 Three types of perovskite solar cell (from left to right): TiO_2 nanoparticle based; TiO_2 nanowire based; Planar structure

The perovskite solar cell can be classified into three type based on mesoporous TiO_2 structure: nanoparticle based, nanowire based and planar solar cell. The plot of three different types of structure perovskite solar cell is shown in figure 1.8.

1.3.4.1 Nanoparticle (NP) Structure

The nanoparticle structure, as shown in figure 1.8, is so far the most general type of perovskite solar cell. The perovskite first infiltrated in the mesoporous structure, and then formed pure perovskite cuboid structure on top of the nanoparticle layer.[17] The addition of mesoporous TiO_2 increases the overall conductivity for the perovskite layer because the resistivity of TiO_2 is lower. The film thickness of TiO_2 nanoparticle affects the performance of solar cell. It is reported that as TiO_2 nanoparticle film gets thicker, the fill factor and open-circuit voltage decrease.[12]

The experiments conducted in this thesis are all based on TiO_2 nanoparticle perovskite solar cells.

1.3.4.2 Nanowire (NW) Structure

In TiO_2 nanowire structure, the nanowires replace the nanoparticles. TiO_2 nanowires are grown in a direction perpendicular to the glass substrate. Again, the nanowire length also affects the property of solar cell. As the nanowire length increases, the open-circuit voltage as well as the short-circuit current density decrease and thus results in lower efficiency.[18]

1.3.4.3 Planar Structure

In the case of planar structure perovskite solar cells, as shown in figure 1.8, there is no scaffold TiO_2 nanostructure included. The perovskite crystal structure deposits directly on the n-

type hole-blocking layer. The percent of perovskite layer coverage on the glass substrate significantly influence the performance of the solar cell.

The perovskite layer in planar type cell has a lower conductivity compared with TiO_2 nanoparticle or nanowire type cell since no mesoporous TiO_2 material is added. Also, the space charge polarization effect mentioned in section 1.2.2 is more obvious in planar structure cell because the perovskite layer is formed in between of the p-type and n-type semiconductor.

1.3.5 Degradation

As mentioned in chapter 1.3.1, the stability of perovskite structure is a problem need to be addressed. Oxygen and moisture in the atmosphere can directly affect the stability of the components in reaction.[19] Due to the high sensitivity of $CH_3NH_3PbI_3$ to water, it tends to hydrolyze in the presence of moisture, leading to the degradation of perovskite.[20] However, it should be clarified that moisture, oxygen, UV and evaluated temperature are necessary for the decomposition process. When exposed to these factors, the perovskite structure will undergo the following decomposition reactions:[21]

$$CH_3NH_3PbI_{3(s)} \xrightarrow{H_2O \text{ and heat}} CH_3NH_3I_{(s)} + PbI_{2(aq)} \quad (1.8a)$$

$$CH_3NH_3I_{(aq)} \longrightarrow CH_3NH_{2(aq)} + HI_{(aq)} \quad (1.8b)$$

$$4HI_{(aq)} + O_{2(g)} \longrightarrow 2H_2O_{(aq)} + 2I_{2(s)} \quad (1.8c)$$

$$2HI_{(aq)} \longrightarrow H_{2(g)} + I_{2(g)} \quad (1.8d)$$

Many products of these reactions can hinder the operation of perovskite solar cell. For example, metal halide such as PbI_2 will reduce the performance due to its poor optical property and higher band gap. Furthermore, the presence of CH_3NH_2 as a decomposition product is another

problem. CH_3NH_2 could stay in the perovskite layer and thus influence the photovoltaic processes.[21]

Plenty of researches have been done to show that the degradation of perovskite results from the mixture of these factors. It has been published that the degradation in absorption of $CH_3NH_3PbI_3$ films after exposure to 100 suns for 60 min at elevated sample temperature (~45−55^{0}C) was observed. While no evident degradation was found under the same light exposure condition at lower temperature (~25^{0}C).[23] When the perovskite solar cell is exposed to only one of those factors, the degradation is relatively insignificant. Therefore, the decomposition of perovskite can also be seen as a thermal enhanced process.

Another degradation problem occurs at the hole transporting material layer (HTM). It will be mentioned in section 3.1 that the Li^+ doped spiro-OMeTAD is employed as the HTM due to its superior electric conductivity. However, the Li^+ will start to evaporate when the temperature is around 80^{0}C and lower the conductivity significantly.

In order to prevent the decomposition reaction listed above, the perovskite solar cell should be keep away from the degradation factors such as moisture, high concentration oxygen and high environmental temperature.

1.3.6 Developent of Perovskite Solar Cell

The perovskite has not attracted researchers' attention until recent years. Perovskite was first published to incorporate into solar cell application in 2009.[24] In that research, a thin layer of perovskite was served as the light absorber, while the focus was on dye-sensitized solar cell and acquired a PCE of 3.8%. Nevertheless, the cell was unstable because of the liquid corrosive electrolyte. Since perovskite was sensitive to air and moisture, finding a replacement for the liquid

electrolyte was necessary. Additionally, air, moisture and evaluated temperature should be avoided during the fabrication of perovskite cell.

A breakthrough of perovskite solar cell was reported in 2012 in which the perovskite was stable under the contact with a solid-state hole transporter and did not need the mesoporous TiO_2 layer to transport electrons.[25] The final PCE was about 10%.

Many achievements were published in 2013. Two-step perovskite deposition method was introduced and obtained a PCE over 15%.[15] Later, Liu et al. showed that it was possible to fabricate perovskite solar cells with efficiency more than 15% by thermal evaporation.[26]

In 2014, many new deposition methods with higher PCEs were reported. A PCE of 19.3% was achieved by planar thin-film structure at UCLA.[27] Later, KRICT achieved a new record with a non-stabilized efficiency of 20.1%.

The researches of perovskite solar cell keep soaring in 2015. Nanowire structured perovskite was reported with V_{OC} more than 1 volt and PCE of 14.71%.[28] Furthermore, many works are being conducted and will be reported soon.

Perovskite solar cell is still at the research phase and has not come to the market. However, due to the low cost and easy fabrication, they will increase the application range of solar cells after commercialized.

1.4 CONCENTRATOR SOLAR CELLS

The Concentrator solar cell is a photovoltaic technology that generates electricity from sunlight.[8] Unlike traditional photovoltaic systems, it utilizes mirrors and lens to focus sunlight onto small, but highly efficient solar cells, as figure 1.9 shows. Besides, concentrator solar cell systems often

use solar trackers to further increase their efficiency. However, the concentrated solar power may cause side effects such as large temperature increase and result in efficiency decrease, thus cooling systems are sometimes utilized to maintain the performance. Inorganic silicon based solar cells are the most used solar cells for concentrated solar cell systems due to their stability at high temperature. Ongoing research and development is rapidly improving their competitiveness in the utility-scale segment and in areas of high solar insolation.

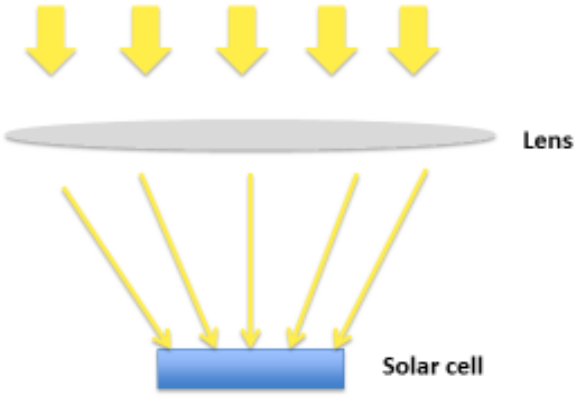

Figure 1.9 Setup of concentrator solar cells

As mentioned in section 1.3.5, perovskite solar cells are vulnerable to high temperature. While researchers want to generate more power by applying concentrator solar cell systems on perovskite solar cells, the evaluated temperature effect that causes degradation in the perovskite solar cell must be taken into concern when designing the concentrator perovskite solar cells. Therefore, in this thesis, the temperature evaluation under different incident solar light intensity was investigated to find out the concentrated solar power range of perovskite solar cell.

1.5 FDTD METHOD AND LUMERICAL FDTD

In this thesis, the simulation of transmittance (%T) and reflectance (%R) of solar cell is done by the LUMERICAL FDTD software in order to figure out the absorbance (%A). The LUMERICAL FDTD is a Finite-Difference-Time-Domain method based software. The basic concept of Finite-Difference-Time-Domain method and the operation interface of LUMERICAL FDTD will be introduced in this section.

1.5.1 Finite-Difference-Time-Domain method

Finite-difference time-domain (FDTD) method is a grid-based numerical analysis technique used for finding approximate solutions to an associated system of differential equations. Since it is a time-domain method, FDTD solutions can cover a wide frequency range with a single simulation run, and treat nonlinear material properties in a natural way.[29] The differential equations are discretized by Finite Difference method. Thus, the basic theory of Finite Difference Method will be introduced in the next section.

1.5.1.1 Finite Difference Method

The finite-difference method (FDM) is an approximation method for solving differential equations. In this method, the Taylor series expansion is used. FDM will be more clearly demonstrated by an example.

First, consider the Taylor series expansion of an ordinary differential equation:

$$f(x_0 + h) = f(x_0) + \frac{f\prime(x_0)}{1!}h + \frac{f^{(2)}(x_0)}{2!}h^2 + \cdots + \frac{f^{(n)}(x_0)}{n!}h^n + R_n(x) \qquad (1.9a)$$

Assume the value of terms with order higher than two are small and can be neglected, then the new equation can be expressed as:

$$f(x_0 + h) \sim f(x_0) + \frac{f'(x_0)}{1!}h = f(x_0) + f'(x_0)h \tag{1.9b}$$

After arrangement, the differential term can be approximated as:

$$f'(x_0) = \frac{f(x_0+h)-f(x_0)}{h} \tag{1.9c}$$

Now, consider an ordinary differential equation as example:

$$u'(x) = 3u(x) + 2 \tag{1.10}$$

Express the differential term by equation (1.8c):

$$u'(x) = \frac{u(x+h)-u(x)}{h} \tag{1.11}$$

Then substitute (1.10) into (1.9):

$$\frac{u(x+h)-u(x)}{h} = 3u(x) + 2 \tag{1.12}$$

After arrangement, the equation can be expressed as:

$$u(x + h) = u(x) + h[3u(x) + 2] \tag{1.13}$$

In this way, once the initial value of $u(x)$ is known, one can obtain the approximate value of $u(x + h)$ and then the term $u(x + 2h)$ can be calculated by $u(x + h)$ and so on. Note that the h here means the step size. Remember in this method, higher order terms are neglected in the Taylor series expansion. If the step size h gets larger, the error increases. However, if the step size is too small, the calculation will take too much time. Thus the chosen of step size is critical in this method. Figure 1.10 shows the graph of finite difference method in a function $y = f(x)$ and step size h.

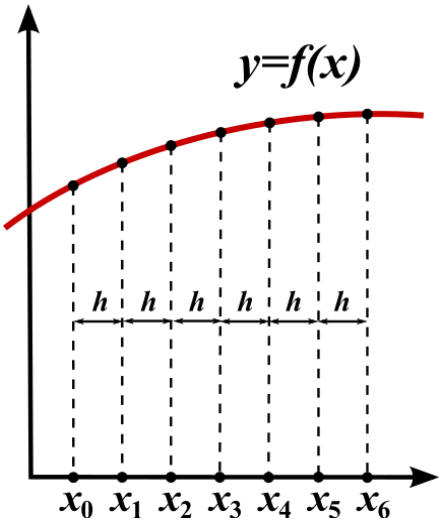

Figure 1.10 The relationship of step size h and function $\boldsymbol{y = f(x)}$[30]

1.5.1.2 Finite-Difference-Time-Domain Method

Finite-Difference-Time-Domain (FDTD) Method was first introduced by Kane Yee, who employed second-order central differences on Maxwell's equations. The steps are showed as follows:[31]

i. Replace all the derivatives in Ampere's and Faraday's laws with finite difference method. Discretize space and time so that the electric and magnetic fields are staggered in both space and time.

ii. Solve the resulting difference equations to obtain "update equations" that express the (unknown) future fields in terms of (known) past fields

iii. Evaluate the magnetic fields one time-step into the future so they are now known (effectively they become past fields)

iv. Evaluate the electric fields one time-step into the future so they are now known (effectively they become past fields).

v. Repeat the previous two steps until the fields have been obtained over the desired duration.

The Yee grid is shown in figure 1.11.

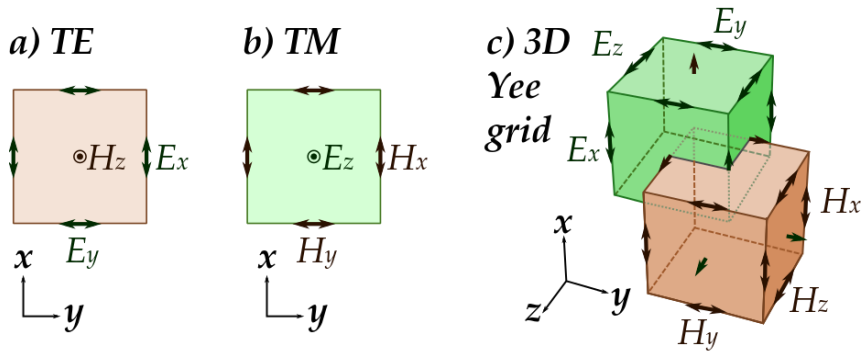

Figure 1.11 Yee Grid[29]

The FDTD steps above basically proceeded the FDM method. But the FDM example showed in section 1.5.1.1 just use one variable along one direction. In the FDTD method, the variables expand to a three dimensional space plus the time domain. However, the processing steps and basic idea are the same.

1.5.2 Lumerical FDTD

The Lumerical FDTD is a high performance 3D FDTD method Maxwell solver for design, analysis and optimization of nanophotonic device, processes and materials.[32] In this thesis, the transmittance and reflectance of a perovskite solar cell structure is simulated in order to calculate the total power absorbed from an incident light. The operation interface of Lumerical FDTD is showed in figure 1.12.

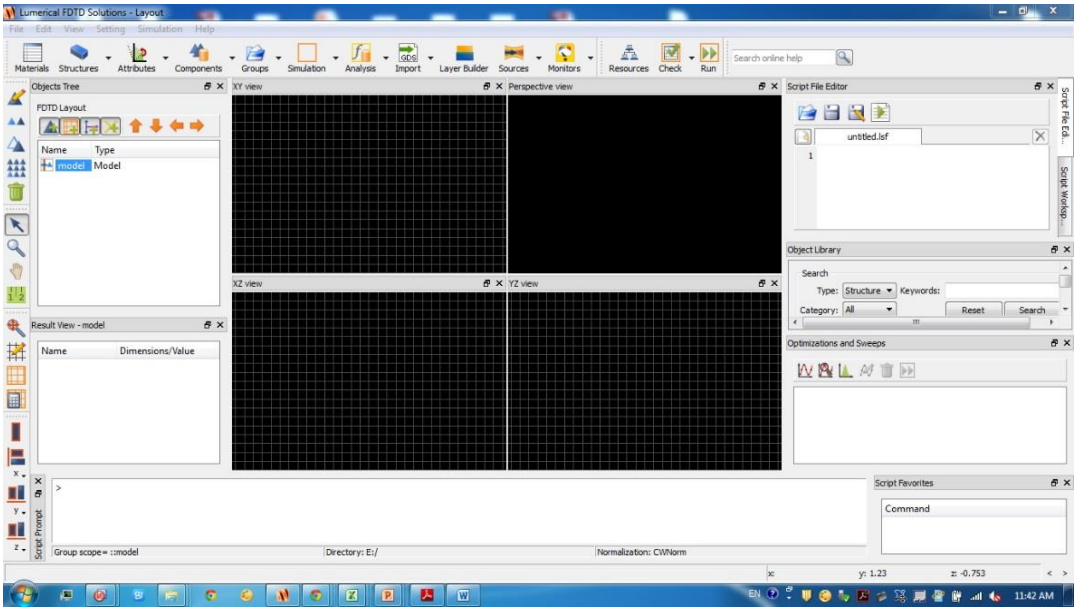

Figure 1.12 Operation interface of Lumerical FDTD

1.6 FINITE ELEMENT METHOD AND ANSYS MECHANICAL

1.6.1 Finite Element Method

The finite element method (FEM) is a numerical technique for finding approximate solutions to boundary value problems for partial differential equations.[33] In modern engineering problems, it often takes lots of time to obtain an exact solution for each problem. Sometimes it is even impossible to get an exact solution. Thus the FEM offers a quicker way to solve problems. FEM subdivides a large problem into smaller parts, called finite elements. In each finite element, the original complex equations are replaced by simpler equations that can offer approximate solution to the original one. Then the simpler equations are assembled to form a set of equations

that describe the entire problem. A simple example will be demonstrated below to show how FEM works.[34]

Consider a function: $f = \int_{-1}^{1}(x^2 + 6)dx$. The graph is showed in figure1.13a. The exact solution is around 12.667. This problem will then be solved with FEM. The first step is to divide the interval of integration into N sections. The second step is to choose a function to approximate the value of $f(x)$ in each section; here a constant function that equals to the value of $f(x)$at the mid-point of each section is chosen. The third step is to multiply the value of constant function by the length of the section to get the approximate integration of $f(x)$ over this section. The final step is to sum up the product of all sections to obtain the approximate solution. Figure1.13 shows the relation of finite element number N and the error.

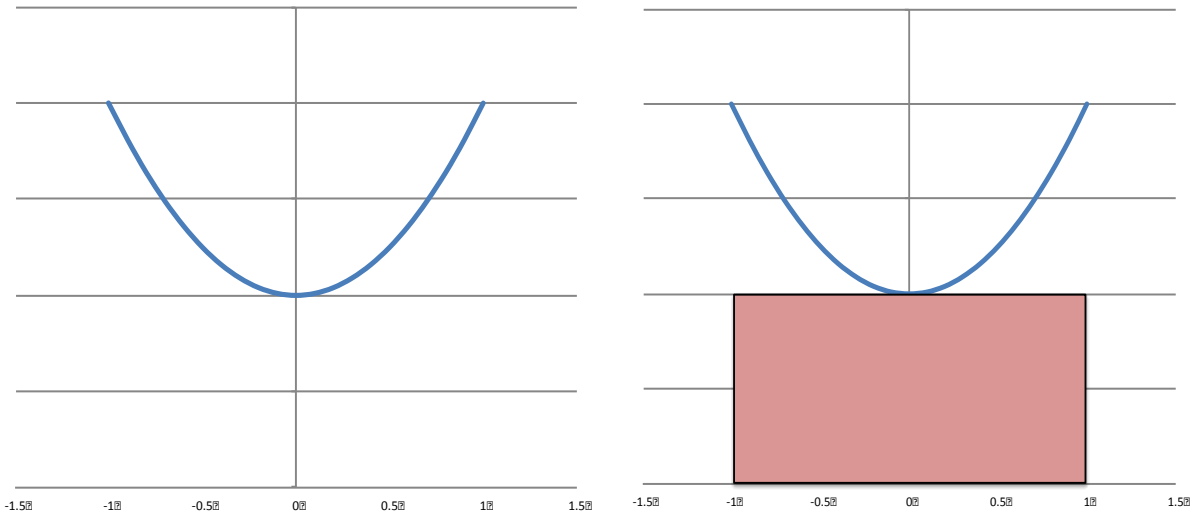

(a) **(b)**

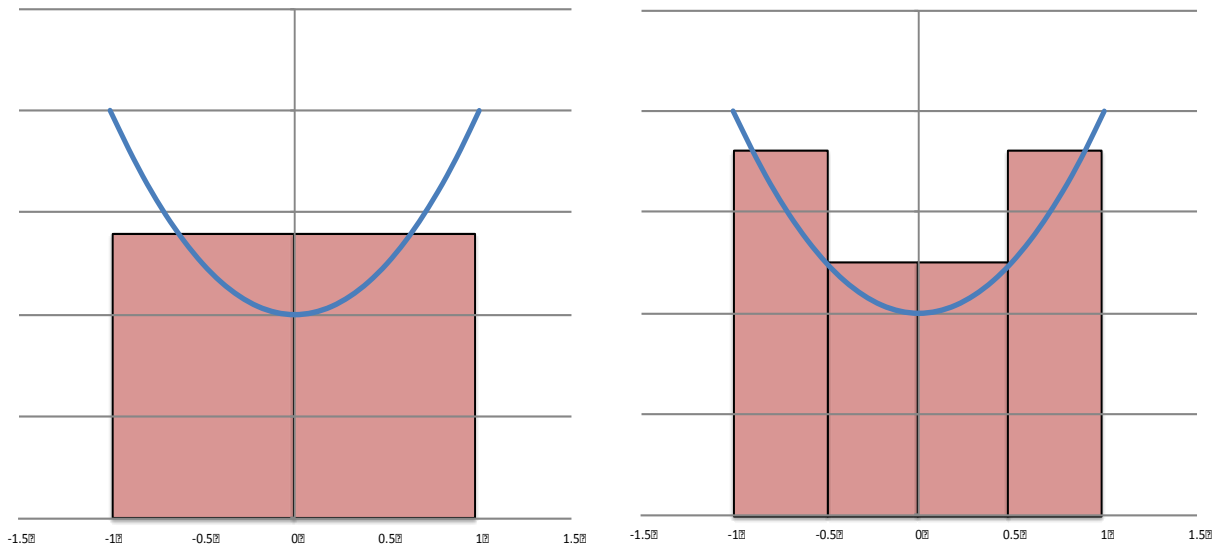

(c) **(d)**

Figure 1.13 (a) the graph of function $\boldsymbol{f = \int_{-1}^{1}(x^2 + 6)dx}$; (b) N=1, value of integration=12, error~5.3%; (c)N=2, value of integration=12.5, error~1.3%; (d) N=4, value of integration=12.625, error~0.33%

By using FEM, the original integral equation has been simplified into a set of rectangular area addition. It can also be noted that as the number of finite elements increases, the error decreases. Therefore, choosing finite elements sizes is a crucial step in FEM.

1.6.2 Ansys Mechanical

ANSYS Mechanical is a finite element method based software for structural analysis, including linear, nonlinear, dynamic hydrodynamic and explicit studies.[35] This computer simulation product uses finite elements to model a wide range of mechanical design problems. It also covers thermal analysis and coupled-physics that involves piezoelectric, acoustics, and thermo-electric analysis. In this thesis, the heat transfer and temperature change of the glass substrate in the

perovskite solar cell under different level of incident solar light are calculated by the use of ANSYS Mechanical. The operation interface of Ansys Mechanical is showed in figure 1.14.

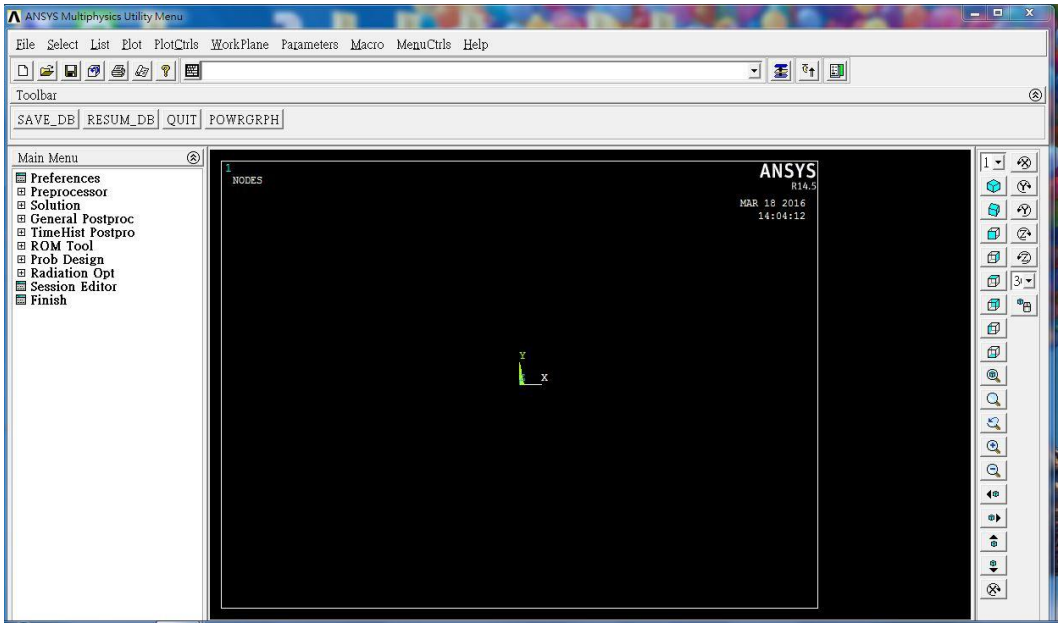

Figure 1.14 Ansys Mechanical operation interface

2.0 REAEARCH DESCRIPTION

2.1 MOTIVATION AND OBJECTIVE

While perovskite solar cell is considered as a potential photovoltaic device, it undergoes decomposition when exposed to moisture, oxygen, UV and evaluated temperature. Many researches have been conducted to investigate the effects of these factors. Most of them characterize one factor at a time. The temperature effect, for instance, is controlled when conducting the measurement of different light intensity. However, in practice, part of the incident light energy will be absorbed by the glass substrate and be converted into heat, resulting in temperature raise. For modern solar cell arrangement, the solar light is often concentrated by lens to get better performance from small area of cell. In this case, the temperature evaluation will be even higher and thus cause severe degradation in perovskite solar cell. A question is at which incident light condition the degradation of perovskite solar cell become significant. In this thesis, the performance of perovskite solar cell under different temperature were measured and the temperature change of glass substrate under different incident light intensity were simulated by software. The best range of light intensity for operating perovskite solar cell was found by figuring out the relation between incident light intensity, temperature change and perovskite solar cell performance.

2.2 TASKS

The first task is to measure I-V curve and Incident-photon-to-current efficiency (IPCE) of perovskite solar cell to check the performance of perovskite solar cells. Second, the transmittance and reflectance of perovskite solar cell from 200nm to 4000nm are modeled by Lumerical FDTD software. And then the total absorbed power for the solar cell under specific incident light can be obtained by subtracting the reflected and transmitted parts. The third job is to simulate the temperature evaluation under different power input by using Ansys Mechanical software and characterize the relation between temperature increase and incident light intensity. The final task is to conduct the I-V curve and IPCE measurement under different temperature in order to understand the performance regarding the temperature effect.

3.0 EXPERIMENTAL DETAILS

3.1 TIO_2 NANOPARTICLE PEROVSKITE SOLAR CELL FABRICATION

In this section, the fabrication of TiO_2 nanoparticle based perovskite solar cell will be briefly introduced since the experiments conducted in this thesis are all based on nanoparticle perovskite solar cell.

3.1.1 FTO Glass Substrate

The 2.3mm thick NSG TEC^{TM} 8 FTO glass with 8Ω/sq resistivity was chosen as the substrate for TiO_2 nanoparticle based perovskite solar cell for its good transmittance and conductivity. The FTO glass was cut into 20mm×20mm size pieces. One side of the substrate is etched by acid to erase the FTO conductive layer in order to avoid current leakage. The etching area is used as the anode.

3.1.2 N-Type Electron Transporting Layer (Hole Blocking Layer)

The etching side of the FTO glass substrate was then blocked by kepton tape to prevent n-type material coated on this area. The solution 0.5 mol/L titanium diisopropoxide bis(acetylacetonate) in 1-butanol is spin coated on the rest area to form the n-type material with around 5nm thickness.

The $TiCl_4$ treatment is then utilized to flat the surface and stuff the pores of electron transporting layer formed during the spin coating.

3.1.3 TiO_2 Mesoporous Layer

The TiO_2 nanoparticle paste (Dyesol) is dissolved into ethanol (200proof) to form the TiO2 mesoporous solution. This solution is also spin coated to form mesoporous TiO_2 nanoparticle layer on the ETL. The thickness of this layer is approximately 200 nm.

3.1.4 Perovskite Layer Fabrication by Two Step Method

In the two step method (sequential deposition), The PbI_2 is first deposited on the substrate, and then CH_3NH_3I solution is dipped into the substrate to form $CH_3NH_3PbI_3$ perovskite structure.[15] Firstly, PbI_2 is dissolved in DMF to form a 1mol/L concentration solution. Then the PbI_2 solution is spin coated on the substrate. Second, methylammonium iodide (MAI) is dissolved in isopropanol with concentration of 7 mg/ml. The MAI solution is also spin coated on the previously prepared substrate sample to synthesis the perovskite layer with thickness around 200nm.

3.1.5 Hole Transporting Material

1% Li^+ doped spiro-OMeTAD is employed as the p-type material. Spiro-OMeTAD builds a structure for hole transporting. By doping Li^+, the conductivity and hole mobility are dramatically increased.[36] This material is spin coated on perovskite substrate prepared in last step and the thickness is about 10nm.

3.1.6 Au Electrode Deposition

Au is used as electrodes for the solar cell. It is deposited on both FTO area to produce anode and perovskite side to produce cathode. Electron beam deposition method is utilized to form the electrode layer. High intensity electrons shoot on the gold. Gold will generate high intensity beams shooting on the target deposition area, forming evenly deposited surface. During deposition, a mask is used to control the area of electrode. The thickness of Au layer is approximately 80nm. The side view plot and finished sample are showed on figure 3.1.

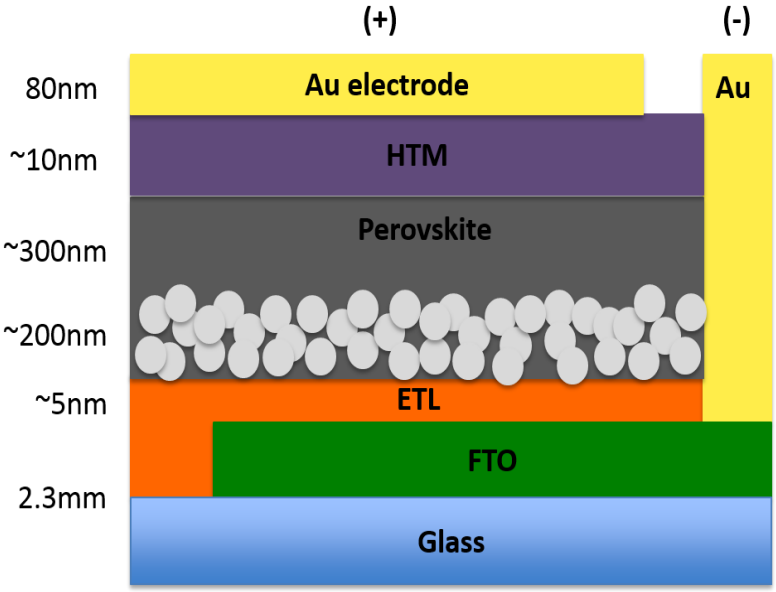

Figure 3.1 Plot of TiO_2 nanoparticle perovskite solar cell structure

3.2 I-V CURVE MEASUREMENT

The I-V (current-voltage) curve of a solar cell demonstrates its energy conversion capability under a standard illumination and temperature. Therefore, the curve describes a set of combinations of current and voltage at which the solar cell can be operated.

In the measurement, a solar simulator is utilized to measure the I-V curve of perovskite solar cell. Solar simulator produces light similar to sunlight, which contains ultraviolet (UV), visible and infrared (IR) light. The generated light is normally set to 1 sun condition (AM1.5G or $1000W/m^2$) in order to eliminate the effect of light intensity and shines on the tested sample. The adjustment of light intensity from solar simulator is done by measuring the I-V curve of a standard reference silicon solar cell. Since the I-V curve of reference silicon cell under 1 sun condition is already known, the light intensity of solar simulator can be modulated by matching the measured I-V curve to the standard curve under 1 sun condition.

In the I-V measurement, the sample cell is connected to a continuously changing external applied voltage. The current through the cell as well as the voltage across the cell are recorded. The I-V curve is done by plotting the corresponding current and voltage. In practical, the current term is usually divided by the solar cell active area to eliminate the effect of area. Thus, the J (current density)-V curve is used more frequently.

In this thesis, the I-V curve was measured under different temperature condition to characterize the performance of perovskite solar cell. A heater was placed on the opposite side of illumination to control the temperature. The circuit of I-V curve measurement and the typical I-V curve as well as the power output of solar cell are shown in figure 3.2 and 3.3 respectively.

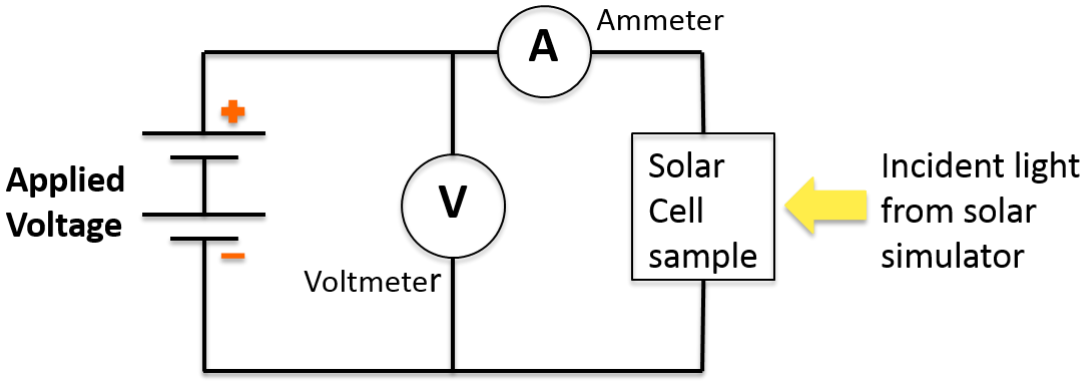

Figure 3.2 Sketch of I-V measurement circuit

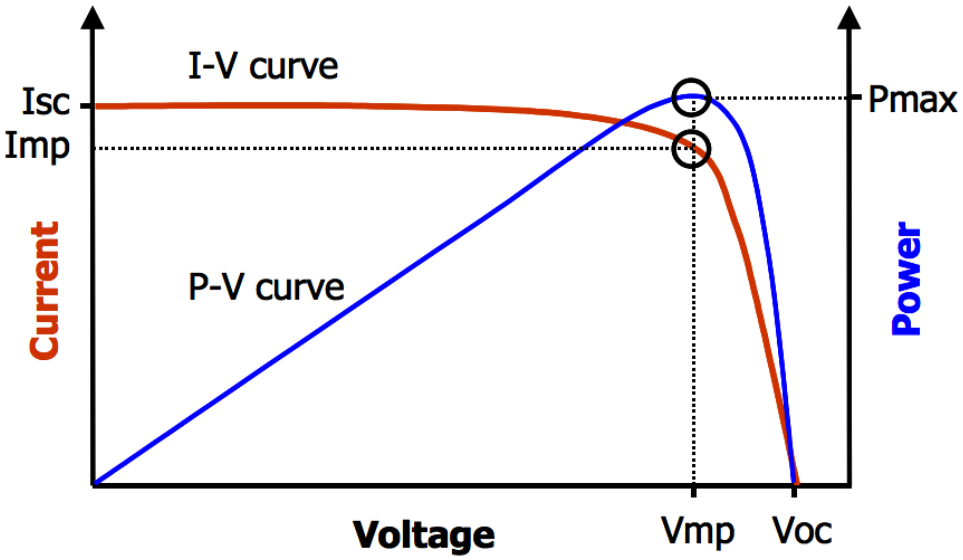

Figure 3.3 Typical J-V curve and power output of solar cell[37]

3.3 INCIDENT PHOTON TO CURRENT EFFICIENCY (IPCE)

Incident photon-to-current efficiency (IPCE) is a technique used to measure the photocurrent generated by solar cell under different wavelength, thus IPCE is a function of wavelength. It is

defined as the number of excited electrons entering external circuit over the number of incident photons. The setup of IPCE measurement is shown in figure 3.5.

In the IPCE measurement, the Xenon lamp is used as the light source. The monochromator is connected to the Xenon lamp in order to filter out the specific wavelength of light. Only one wavelength of light will shoot on the sample cell at a time, thus the IPCE under a specific wavelength can be calculated. During the measurement, the wavelength of light changes continuously and the anode and cathode of the solar cell were connected to the detector with a cable. The detector can read photocurrent data and transfer to computer. Therefore, the photocurrent of solar cell under different wavelength of light is recorded and can be further computed. The formula is already shown in equation 1.4.

The IPCE measurement can be classified into two modes, direct current (DC) mode and alternative current (AC) mode. In DC mode, the incident light shoots on the solar cell while changing the wavelength continuously just as mentioned above. On the other hand, in AC mode, a light chopper is placed in front of the light source. The chopper blocks the light at a preset frequency ranging from 1 HZ to 99 HZ and thus produces an intermittent incident light. The incident light intensity difference between DC and AC mode is demonstrated in figure 3.4.

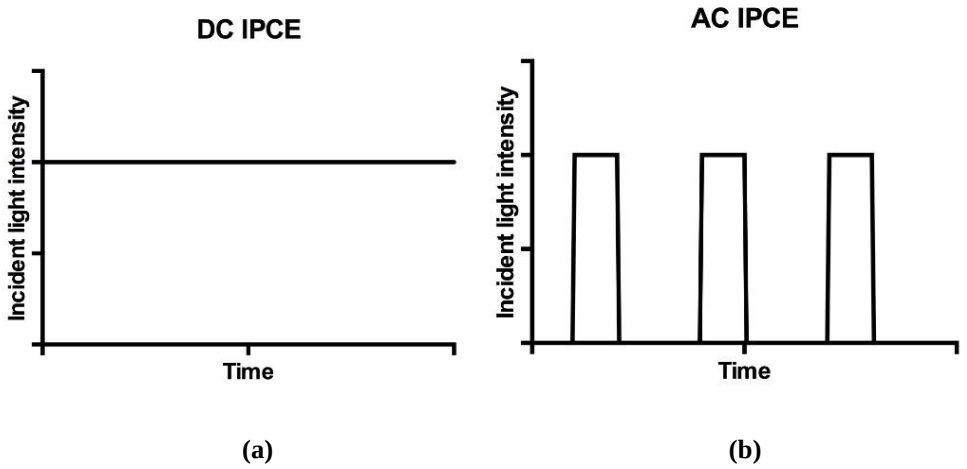

Figure 3.4 (a) DC mode incident intensity (b) AC mode incident light intensity

The photocurrent of solar cell can achieve steady state while the AC mode IPCE is working at lower frequency since the time interval between open and close of the chopper is still long enough. However, as the frequency raises, the time interval gets shorter and shorter. Finally, the time interval of illumination is not long enough for the solar cell to reach steady state and the value of photocurrent decreases. Thus, normally the shape of IPCE curve would decrease as the frequency increase for the same solar cell.

In this thesis, both DC and AC mode IPCE are measured under different temperature condition. Like the I-V curve measurement, the heater is attached to the perovskite solar cell on the opposite side of illumination to control temperature. The effect of temperature on the performance of perovskite solar cell will be further investigated in the result and discussion chapter.

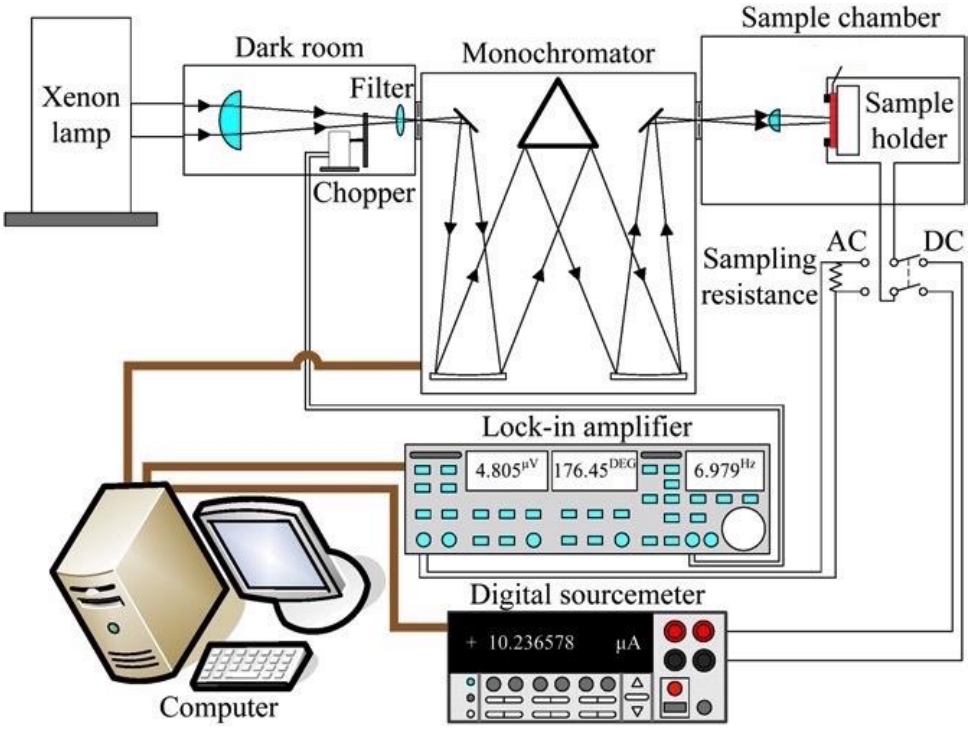

Figure 3.5 Sketch of IPCE Measurement setup[9]

3.4 LUMERICAL FDTD SOFTWARE

In this thesis, the transmittance and reflectance of perovskite solar cell structure with glass, TiO_2 and perovskite layer is simulated to calculate the total power absorbance upon an incident light. Here, the p-type and n-type material are neglected. Since their thickness are relatively thin compared with other layers and are not considered to have significant effects on the optical properties.

To simulate the transmittance and reflectance, some material constants such as complex refractive index should be found and input into the FDTD simulation model. The input light source is a plane wave source with wavelength ranging from 200nm to 4000nm. Two sensors are set in the model, one is behind the light source to record the reflected light energy and the other one is placed underneath the solar cell model to record the transmitted energy. The sketch of simulation model setup and structure built in Lumerical FDTD are shown in figure 3.6 and 3.7.

After the reflectance (R%) and transmittance (T%) are obtained, the power absorbance (A%) can be calculated by A%=100%-R%-T%. Then the total absorbed power spectrum under AM1.5G condition can be obtained by multiplying the standard AM1.5G solar spectrum by A%.

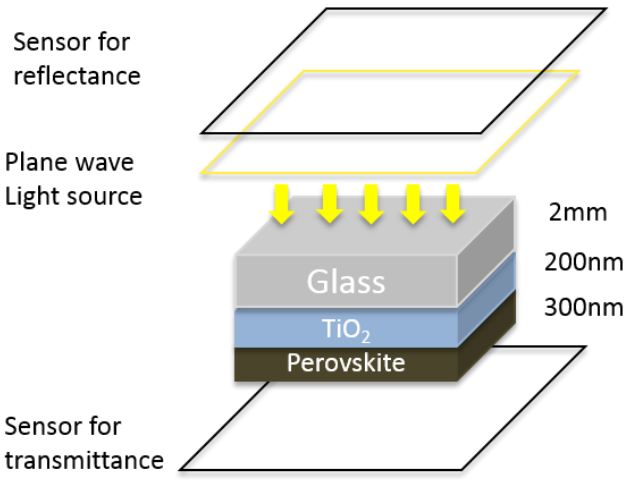

Figure 3.6 Setup of transmittance and reflectance simulation model

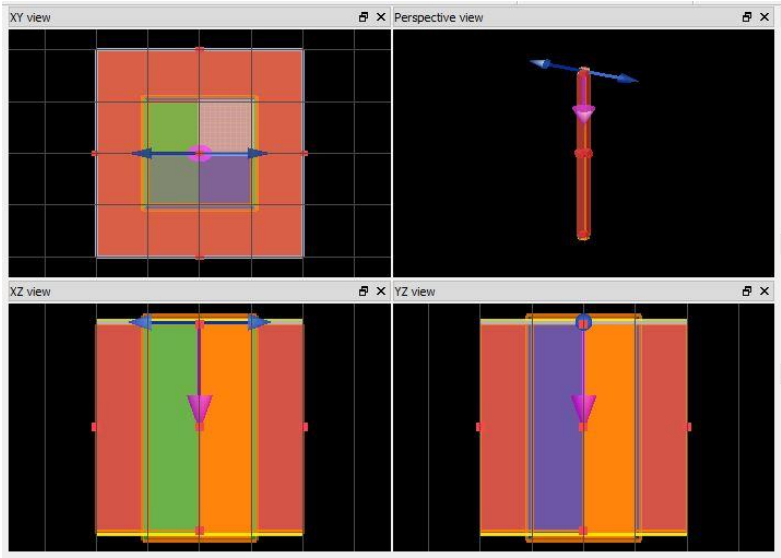

Figure 3.7 Simulation model made in Lumerical FDTD

3.5 ANSYS MECHANICAL

In this thesis, the total power absorbed by the solar cell is then divided into 2 parts. One part contributes to the electric power, the other part contributes to the heat source and cause temperature increase.

Here, an assumption is made, the light with wavelength shorter than 800 nm is mainly absorbed by perovskite and TiO_2 layer and transferred into electric power. For light with wavelength longer than 800 nm, the light power is mainly absorbed by glass substrate and transferred into heat. This is because of two different mechanism of light absorption. When the incident photon contains more energy than the band gap, the material observes light by electron excitation. On the other hand, material observes light primarily by phonon generation when the incident photon contains less energy than the band gap. For perovskite, the band gap energy is approximately equal to the energy contained in the photons with wavelength of 800 nm. While for

glass, the band gap energy is close to the energy of photons with 250 nm wavelength. However, the AM1.5G solar spectrum contains almost no photons in the range below 250 nm. Furthermore, the glass is almost transparent from 250 nm to 800 nm, which means the glass did not absorb light in this range. Thus, perovskite is assumed to absorb all photon energy below 800nm.

When the wavelength is more than 800nm, both materials observe light with phonon generation. Nevertheless, the material needs to be thick for phonon generation to occur. In the case of perovskite, the thickness is not enough and thus phonon generation is assumed to happen only in the 2 mm thick glass layer. The sketch of two light absorbing mechanism range is shown in figure 3.8.

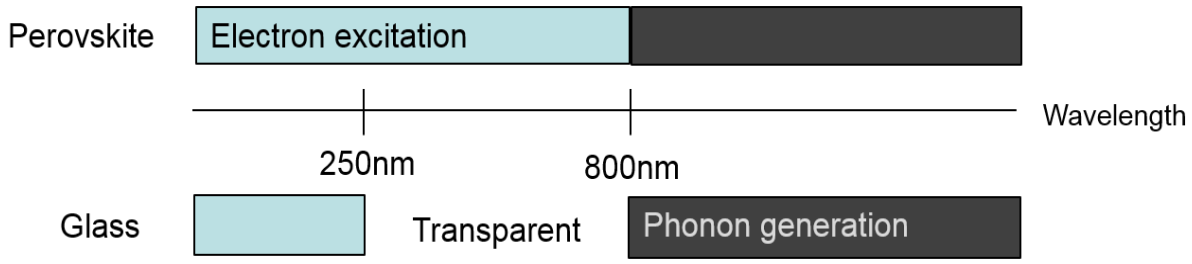

Figure 3.8 Light observing mechanism of perovskite and glass

The Ansys simulation model is showed in figure 3.9. Since it is a one dimensional heat transfer problem and the shape of glass is symmetrical, a simpler 2D model is utilized. Only glass layer is modeled in the heat transfer simulation since glass is much thicker than other layers and also it is assumed that only the power absorbed by glass will be transferred into heat.

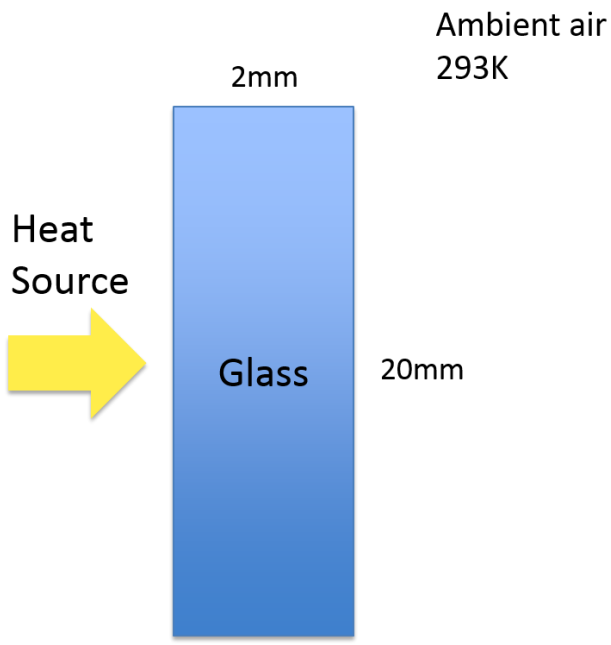

Figure 3.9 Sketch of Ansys simulation model

The initial temperature of the glass substrate is set to be 293K and the ambient air is set to have a constant temperature of 293K. The heat source is applied on one side of the glass substrate and the glass also has heat conduction with the ambient air. The heat source is obtained by integrating the power absorption spectrum from 800nm to 4000nm. The temperature change under different sun conditions are calculated with this model. The correlation of temperature-light intensity is obtained.

4.0 RESULTS

4.1 PHOTON-ELECTRON CONVERSION OF PEROVSKITE CELLS

Figure 4.1 shows the SEM image and photo of a TiO_2 nanoparticle perovskite solar cell used in the experiments of this thesis. Each layer of perovskite solar is marked in the SEM image.

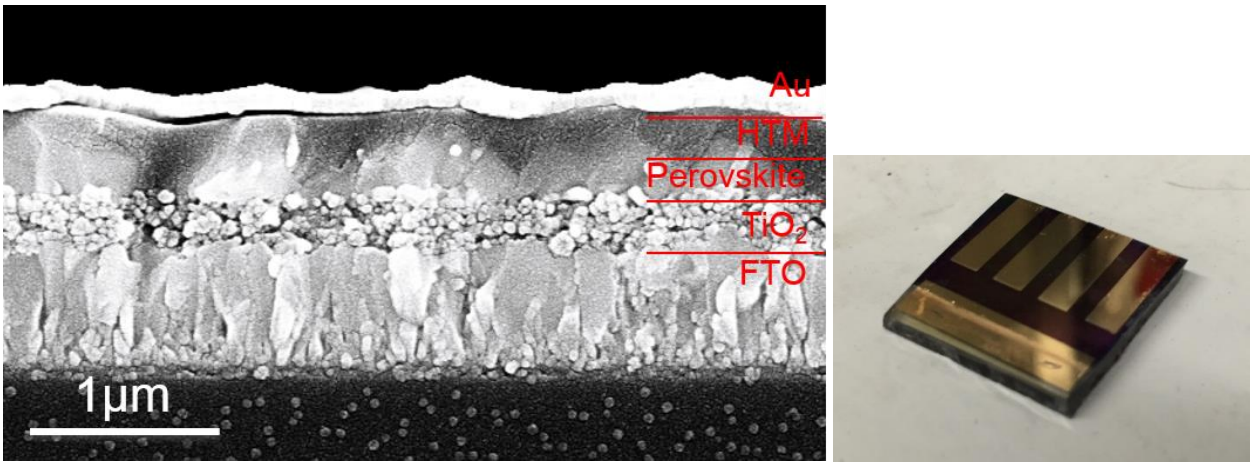

Figure 4.1 SEM image and photo of perovskite solar cell

Next, the I-V curve and incident-photon-to-current efficiency (IPCE) were measured to demonstrate the property of perovskite solar cell. Figure 4.2a shows the I-V curve of the mesoporous TiO_2 nanoparticle based perovskite solar cell with achieved PCE of 15.24%. The IPCE result is shown in figure 4.2b.

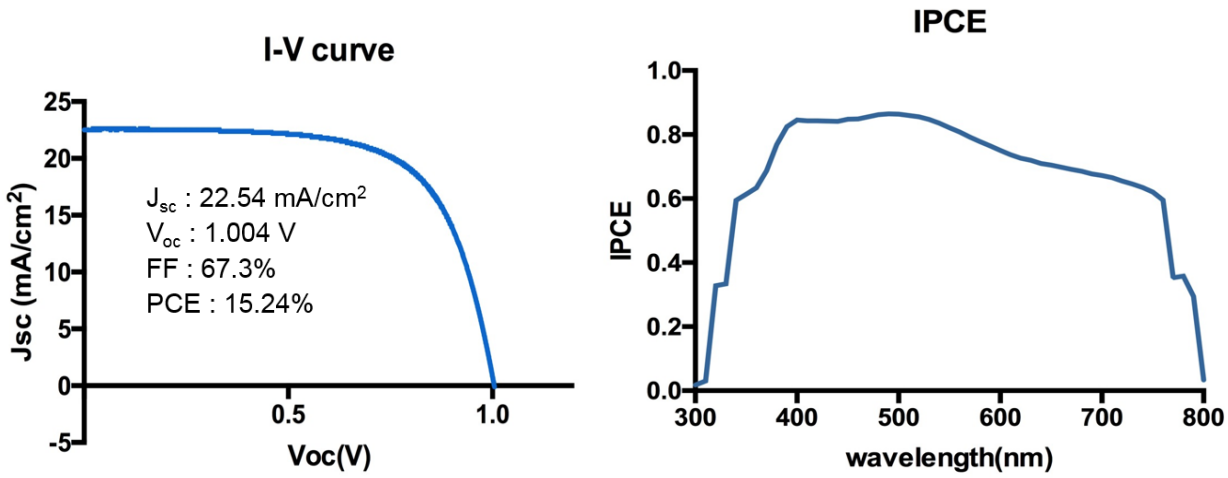

(a) **(b)**

Figure 4.2 (a) I-V curve of perovskite solar cell; (b) IPCE result of Perovskite solar cell

Figure 4.3[38] shows the I-V curve and IPCE result of a typical dye-sensitized solar (DSC) cell for comparison. DSC is another type of thin film solar cell with low cost and thus attracts much interest. However, even the DSC has been studied for decades since its first presence in 1990s, the PCE record was already surpassed by the perovskite solar cell, which has its first report in 2009. The performance comparison is showed in table 4.1.

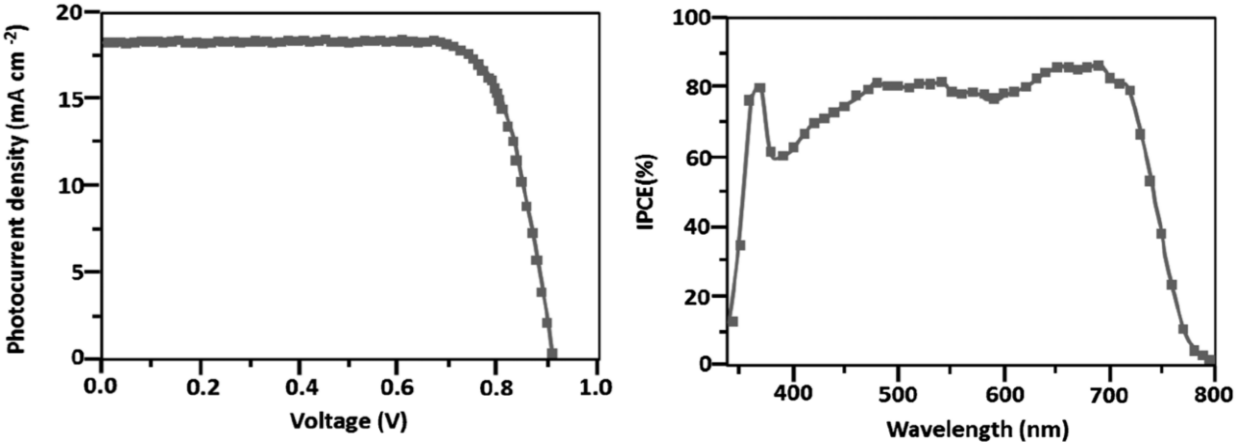

(a) **(b)**

Figure 4.3 (a) I-V curve of DSC; (b) IPCE of DSC

Table 4.1 Performance comparison of perovskite solar cell and dye-sensitized solar cell

	PCE%	J_{sc}	V_{oc}	FF%
Perovskite solar cell	15.24%	22.54 mA/cm^2	1.004 V	67.3%
Dye-sensitized solar cell	13%	18.1 mA/cm^2	091 V	78%

4.2 AC IPCE RESULT

The AC IPCE result for TiO_2 nanoparticle perovskite solar cell under room temperature is demonstrated in this section, as showed in figure 4.4. The frequencies for testing are DC (can be seen as 0 Hz), 1 HZ, 10 HZ, 30 HZ, 50 HZ, 75 HZ, and 95 HZ. It was mentioned in section 3.3 that as the frequency increases, the IPCE would decrease since the time of each light-exposing interval is too short for the perovskite cell to reach steady state.

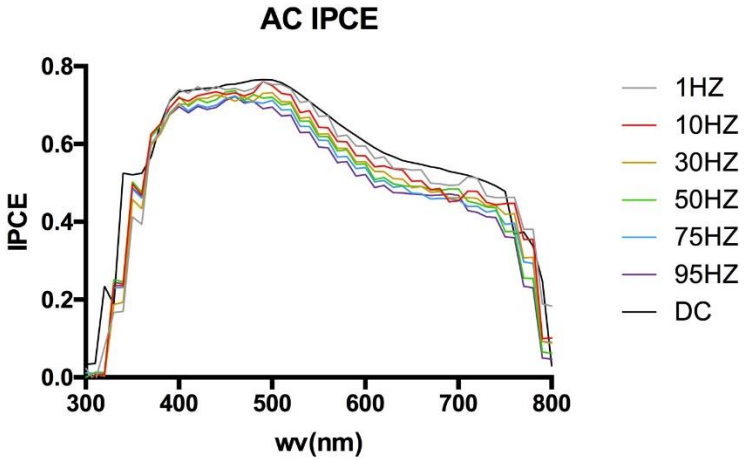

Figure 4.4 AC IPCE result at room temperature

When exposed to light, the perovskite solar cell needs a period of time for the photocurrent to reach steady state, as shown in figure 4.5. This is called response time. In the DC mode, the

perovskite solar cell is under constant illumination and therefore it is always in steady state. However, in AC mode, the time of light-exposing interval gets shorter as frequency increases. When the light-exposing interval gets shorter than the time needed for perovskite cell to reach steady state, the photocurrent would decrease as shown in the AC mode IPCE.

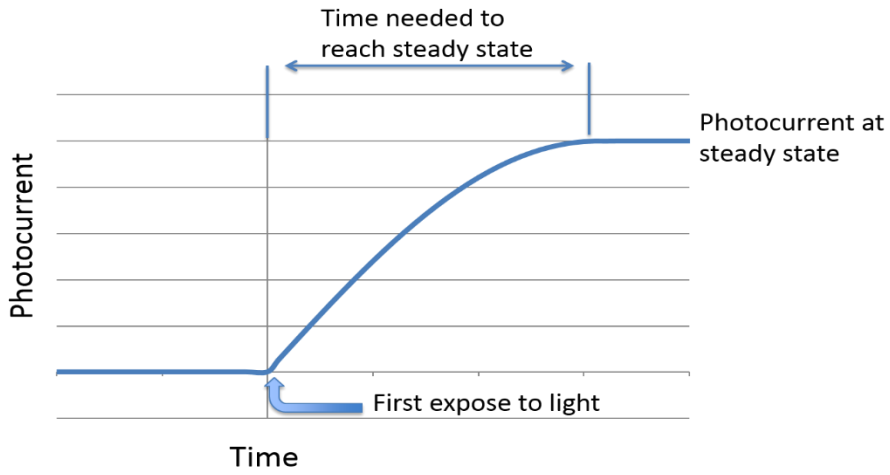

Figure 4.5 Schematic diagram for the response time of perovskite solar cell

4.3 SIMULATION ON INTENSITY-TEMPERATURE CORRELATION

In this section, the temperature increase under different incident light level was being simulated. First, the absorbance was calculated to obtain the total power absorption under each incident light level. Second, part of the absorbed power would be converted into heat source. The heat transfer and temperature change was simulated to acquire the relation between incident light and temperature change.

4.3.1 Simulation of light absorption by Perovskite Solar Cells

Figure 4.6 shows the transmittance and reflectance from 200 nm to 4000 nm of the structure model mentioned in section 3.4.

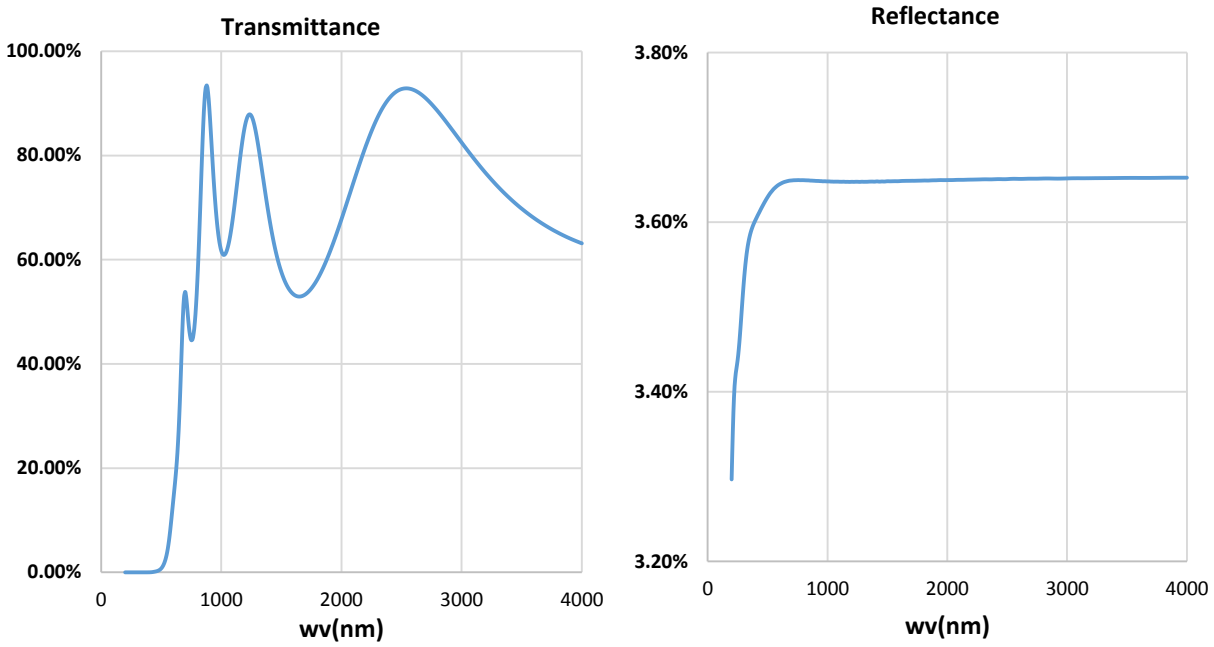

Figure 4.6 Transmittance and reflectance simulation result

When an incident light hits a material, it will either be reflected, absorbed or transmited. Thus the total absorbed energy percent is calculated by $A\% = 100\% - R\% - T\%$. The total A% is showed in figure 4.7(a) and the A% * AM1.5G standard solar spectrum is showed in figure 4.7(b). While the AM1.5G solar spectrum refers to 1 sun condition, the 2 sun condition is simply multiply the 1 sun spectrum by 2, 3 sun is multiplied by 3 and so on.

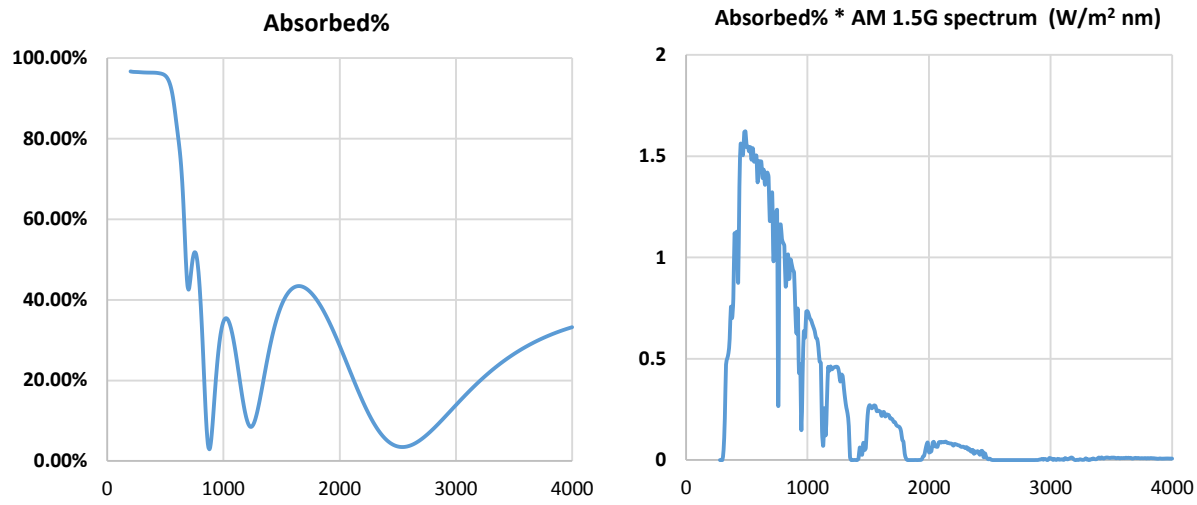

Figure 4.7 (a) Absorbance%; (b) Absorbance%*AM1.5G spectrum

The absorbed power spectrum (figure 4.7b)) will be used to calculate the heat source in the next section. As the assumption stated in section 3.5, the integration from 800nm to 4000nm will be utilized as the heat source and the integration power from 0nm to 800nm will be contributed to electric power.

4.3.2 Temperature increase under concentrated light

The Ansys results are showed in figure 4.8. The model is demonstrated in section 3.5 with the heat source applied on the left hand side of the glass substrate. The temperature change under different incident light intensity of 1 sun, 2 suns, 5 suns and 10 suns are demonstrated below. The setup of the model is displayed in figure 3.9. The initial condition of the glass substrate is set to be 293K (20^0C) and the ambient gas is air with constant temperature 293K (20^0C). The simulation results show the final temperature of glass substrate under different light intensity at steady state. Based

on the simulation results, the temperature of glass substrate under different incident light intensity was found. The results of different incident light intensity and correlated temperature is showed in table 4.2.

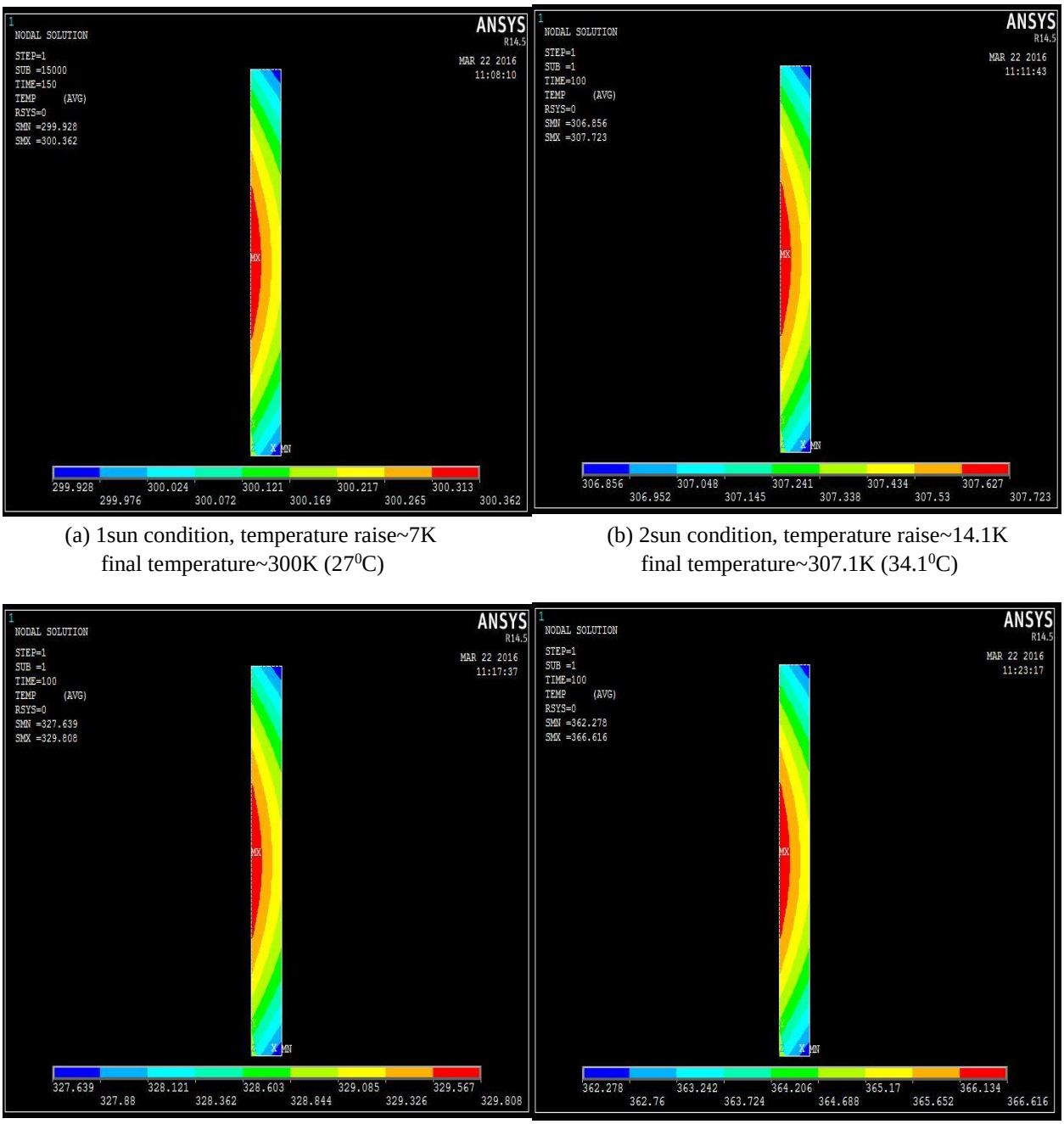

(a) 1sun condition, temperature raise~7K final temperature~300K (27^{0}C)

(b) 2sun condition, temperature raise~14.1K final temperature~307.1K (34.1^{0}C)

(c) 5sun condition, temperature raise~35.4K final temperature~328.4K (55.4^{0}C)

(d) 10sun condition, temperature raise~70.7K final temperature~363.7K (90.7^{0}C)

Figure 4.8 Temperature evaluation results in Ansys Mechanical

Table 4.2 Temperature evaluation under different incident light level

Incident light intensity	1 sun	2 suns	3 suns	4 suns	5 suns	6 suns	7 suns
Final temperature	~300.1K	~307.1K	~314.2K	~321.3K	~328.4K	~335.4K	~342.5K
Incident light intensity	8 suns	9 suns	10 suns	12 suns	14 suns	16 suns	18 suns
Final temperature	~349.6K	~356.7K	~363.7K	~377.9K	~392K	~406.2K	~420.3K

4.4 ANALYSIS OF INTENSITY-TEMPERATURE DEPENDANCE EFFECT

In this section, the I-V curve and AC IPCE were measured under different temperature to find out the performance under different incident light intensity.

4.4.1 I-V curve under different temperature

The I-V curve measured under 30^0C, 40^0C, 50^0C and 60^0C temperature condition are showed in figure 4.9 to characterize the temperature effect. The characteristics are shown in table 4.3.

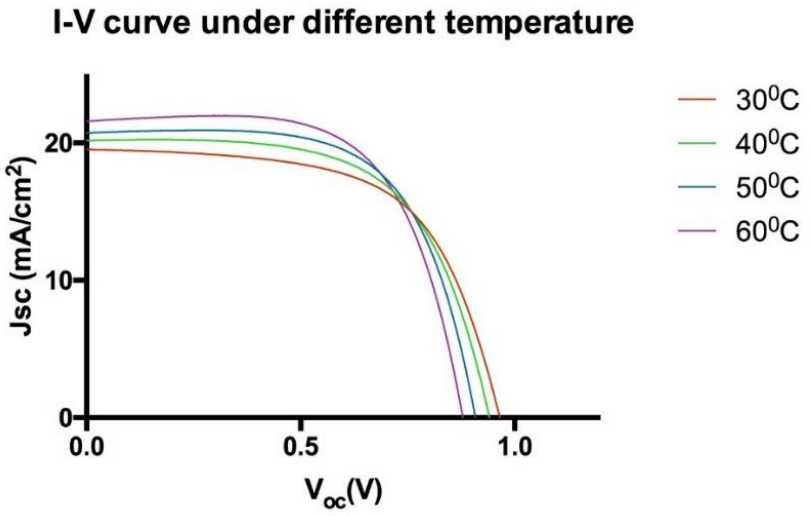

Figure 4.9 I-V curve under different temperature

Table 4.3 I-V curve characteristics under different temperature

	J_{sc} (mA/cm^2)	V_{oc} (V)	FF (%)	PCE (%)
30^{0}C	19.53 mA/cm^2	0.965 V	61.14 %	11.52 %
40^{0}C	20.19 mA/cm^2	0.941 V	62.34 %	11.84 %
50^{0}C	20.71 mA/cm^2	0.908 V	64.95 %	12.22 %
60^{0}C	21.57 mA/cm^2	0.878 V	65.24 %	12.36 %

It can be seen in figure 4.9 that the V_{oc} decreases as the temperature raises. However, the increased J_{sc} and FF cancels the V_{oc} defect and result in an improved PCE.

4.4.2 IPCE under different temperature

The IPCE results will be compared under the same frequency with different temperature (from room temperature to 80^{0}C) in this section. The frequencies are DC (0HZ), 10HZ, 30HZ, 75HZ, as shown in figure 4.10.

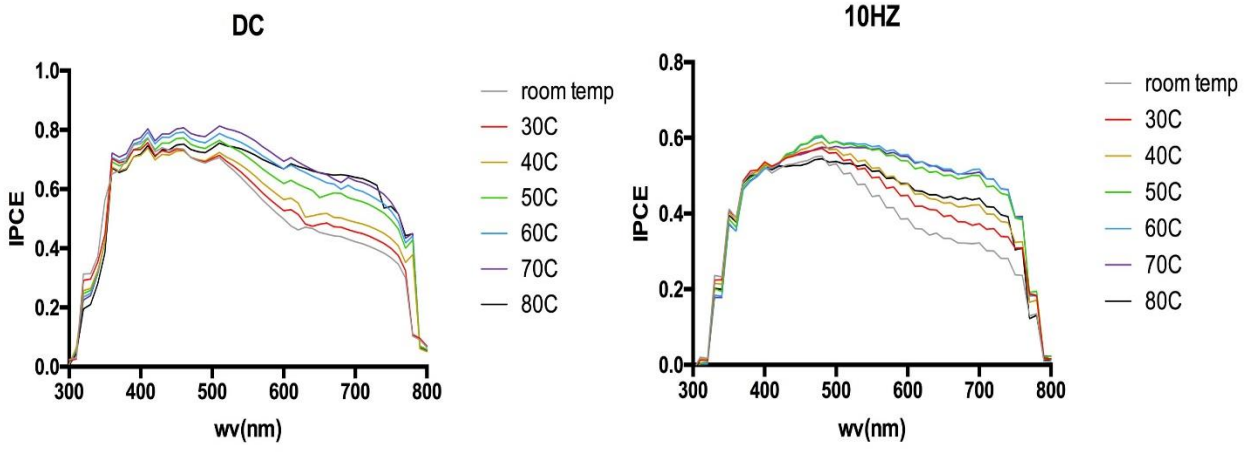

(a) **(b)**

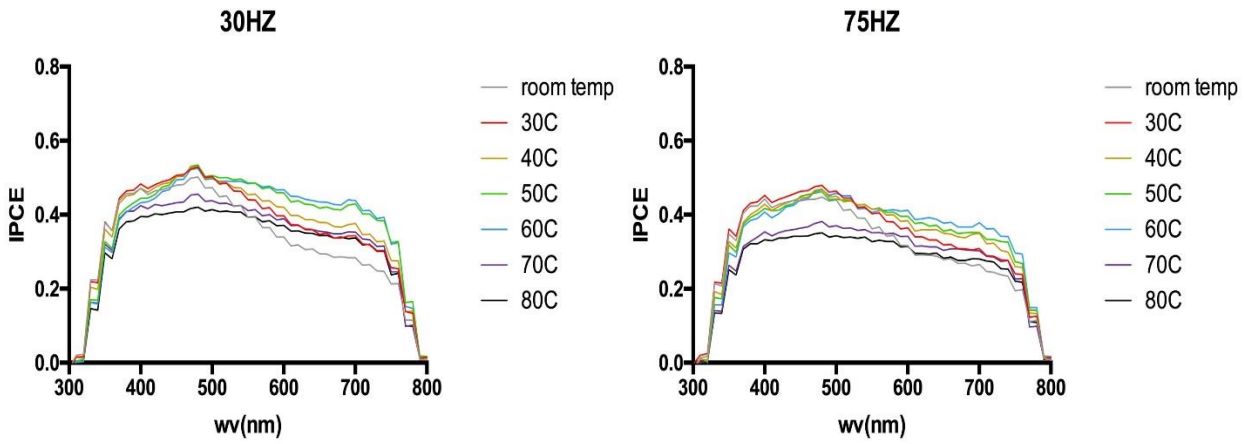

(c) **(d)**

Figure 4.10 IPCE under same frequency with different temperature

Figure 4.10 shows that as the temperature increases, the IPCE results also increase no matter in DC or in different frequency AC mode. This can be explained by the mobility change of TiO_2 mesoporous layer. When an incident photon hits the perovskite layer and generate an electron-hole pair, the electron needs to travel through the perovskite layer in order to reach the external circuit. However, during this process, there is a chance for the electron to recombine with the hole and thus this electron will not contribute to the photocurrent. The function of mesoporous TiO_2 layer here is to transport the electrons. As the temperature rises, the mobility of mesoporous TiO_2 nanoparticle also increases. Thus, the TiO_2 nanoparticles can transport electrons in a faster pace to reach external circuit and lower the chance of recombination.

Another fact that can be observed is the temperature enhancing effect is more obvious in longer wavelength region than in short wavelength region. That is, the IPCE result increases more at higher wavelength. This is because of the absorption depth. Photons with higher energy will be absorbed first, which means a shorter absorption depth, and generates an electron-hole pair closer to the n-type material. As mentioned in section 1.1, photons with shorter wavelength contain more

energy. So the electrons excited by shorter wavelength photons only need to travel shorter distance to reach external circuit and thus the mobility of TiO_2 at room temperature is enough to transport the electron to the external circuit. In other words, almost all electrons excited by short wavelength photons can enter the external circuit without recombination at room temperature. However, photons with longer wavelength have to travel longer before they can be absorbed and generate electron-hole pair. Thus, electrons excited by long wavelength photons have to travel long distance before they enter external circuit and the mobility of TiO_2 at room temperature is not enough to transport them for so long. Therefore, quite a few electrons recombined before they enter external circuit at room temperature. As temperature increases, the TiO_2 nanoparticles are able to transport electrons faster and decrease the chance of recombination. Thus, more electrons can contribute to photocurrent. The comparison of electrons excited by long and short wavelength photons are showed in figure 4.11.

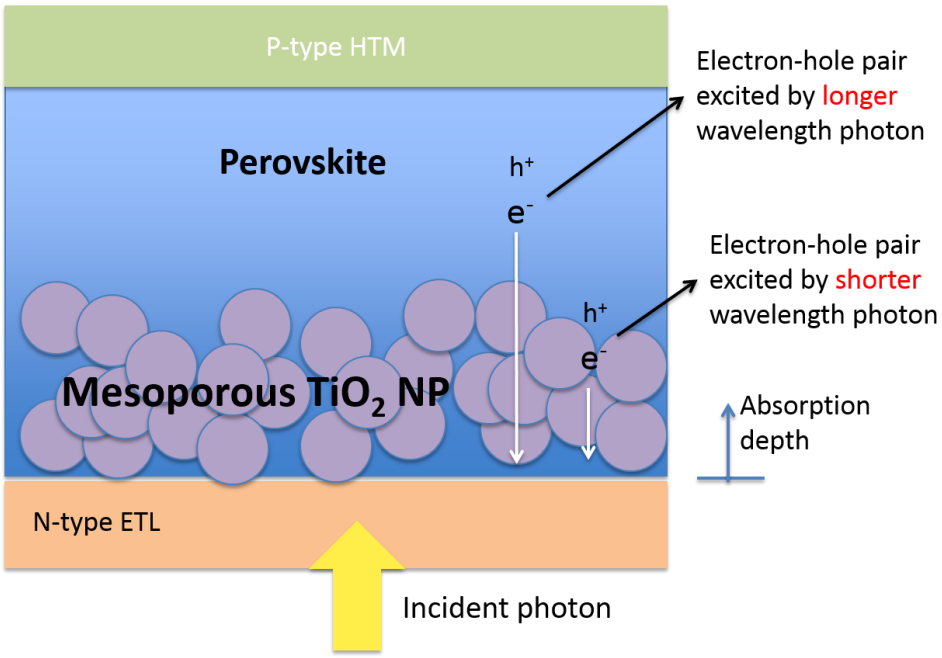

Figure 4.11 Absorption depth comparison

It can also be noted from figure 4.10 that the IPCE result above 70^0C is relatively unstable. It even decreased dramatically at 30HZ and 75HZ IPCE. As mentioned in section 1.3.5, the perovskite layer is sensitive to moisture. Perovskite will react with H_2O and decompose. The evaluated temperature condition can further accelerate this reaction. Therefore, the decrease of IPCE at 70^0C is attributed to the significant degradation of perovskite layer.

Moreover, the decomposition of HTM layer is another issue for the IPCE decrease. The Li^+ doped spiro-OMeTAD was chosen as the hole transporting material because of its superior electric conductivity. But it starts to evaporate when the temperature gets close to 80^0C and reduce the conductivity significantly. Thus, this phenomenon along with the perovskite degradation are responsible for the further drop of IPCE at 80^0C. Thus, it is obvious that at high temperatures, i.e. above 60^0C, either certain fading mechanisms are accelerated or new degradation reactions occur, causing rapid absorber material and device degradation.[21]

5.0 DISCUSSION AND CONCLUSION

The temperature evaluations under different incident light level were simulated. First, the transmittance and reflectance were modeled by Lumerical FDTD software to calculate the absorbance. The absorbance was then multiplied by the AM1.5G solar spectrum to obtain the total power absorbed. Based on the assumption, the energy of photons with wavelength from 800 nm to 4000 nm would be transformed into heat source. Thus, by integrating the total power absorbance spectrum, the input power for heat source under different light intensity was acquired. The temperature evaluation was modeled by Ansys Mechanical with a 2D model. The correlation of temperature-incident light intensity is then obtained as shown in table 4.2.

In the IPCE measurements, the perovskite solar cell displayed higher IPCE under evaluated temperature due to the increased mobility of mesoporous TiO_2 layer. Thus, increasing temperature will improve the performance of perovskite solar cell. However, the improving effect sustained only until 60^0C. After the temperature got over 60^0C, the performance of perovskite cell reduced significantly. This resulted from the instability of perovskite and the HTM layer decomposing at high temperature.

The perovskite undergoes the following reaction when exposed to moisture:[39]

$$[(CH_3NH_3^+)PbI_3]_n + H_2O \rightleftharpoons [(CH_3NH_3^+)_{n-1}(PbI_3)_n][H_3O^+] + CH_3NH_2 \quad (5.1a)$$

$$[(CH_3NH_3^+)_{n-1}(PbI_3)_n][H_3O^+] \rightleftharpoons HI + PbI_2 + [(CH_3NH_3^+)PbI_3]_{n-1} + H_2O \quad (5.1b)$$

In the reactions above, the presence of water is critical and the reaction products will cause further degradation thus impair the performance of perovskite cell. Additionally, it is regarded as a thermal enhanced reaction. Thus, evaluated temperature will accelerate the degradation. The

HTM layer is another issue while the Lithium ion starts to evaporate when the temperature increased to around 80^0C. The evaporation of Lithium ion reduced the conductivity of HTM layer and thus impaired the performance.

At this time, the operation of perovskite solar cell should be controlled under 60^0C to keep the performance. Based on the simulation result, the corresponding light intensity that increases the temperature of glass substrate to around 60^0C is the 5.5 sun condition. Thus, the concentrated solar light intensity for perovskite solar cell should not exceed 5.5 sun.

Many researches have been done to prevent the moisture and temperature problem such as encapsulate the solar cell and some are still proceeding. Besides, the study of HTM layer is still continuing to find out substitute material with better conductivity and stability at high temperature. Therefore, the perovskite solar cell should be able to operate with higher concentrated solar light in the near further.

BIBLIOGRAPHY

[1] G. Turner, "Global Renewable Energy Market Outlook 2013."

[2] "Perovskite solar cell," Wikipedia, the free encyclopedia. 05-Mar-2016.

[3] V. K. Mehta and R. Mehta, Principles of electronics: for diploma, AMIE, degree & other engineering examinations. New Delhi: S. Chand, 2005.

[4] F. Yu, "INTERNAL POLARIZATION EFFECT IN PEROVSKITE SOLAR CELLS," University of Pittsburgh, 2016.

[5] "Formation of a PN-Junction | PVEducation." [Online]. Available: http://pveducation.org/pvcdrom/pn-junction/formation-pn-junction. [Accessed: 09-Mar-2016].

[6] "Dielectric Polarization," chemwiki.ucdavis.edu, 05-Dec-2014. [Online]. Available: http://chemwiki.ucdavis.edu/Core/Materials_Science/Optics/Dielectric_Polarization. [Accessed: 15-Mar-2016].

[7] J. R. Macdonald, "Theory of ac space-charge polarization effects in photoconductors, semiconductors, and electrolytes," Phys. Rev., vol. 92, no. 1, p. 4, 1953.

[8] X.-Z. Guo, Y.-H. Luo, Y.-D. Zhang, X.-C. Huang, D.-M. Li, and Q.-B. Meng, "Study on the effect of measuring methods on incident photon-to-electron conversion efficiency of dye-sensitized solar cells by home-made setup," Rev. Sci. Instrum., vol. 81, no. 10, p. 103106, 2010.

[9] G. Xue, X. Yu, T. Yu, C. Bao, J. Zhang, J. Guan, H. Huang, Z. Tang, and Z. Zou, "Understanding of the chopping frequency effect on IPCE measurements for dye-sensitized solar cells: from the viewpoint of electron transport and extinction spectrum," J. Phys. Appl. Phys., vol. 45, no. 42, p. 425104, Oct. 2012.

[10] M. A. Green, A. Ho-Baillie, and H. J. Snaith, "The emergence of perovskite solar cells," Nat. Photonics, vol. 8, no. 7, pp. 506–514, Jun. 2014.

[11] C. Li, X. Lu, W. Ding, L. Feng, Y. Gao, and Z. Guo, "Formability of ABX 3 (X = F, Cl, Br, I) halide perovskites," Acta Crystallogr. B, vol. 64, no. 6, pp. 702–707, Dec. 2008.

[12] H.-S. Kim, C.-R. Lee, J.-H. Im, K.-B. Lee, T. Moehl, A. Marchioro, S.-J. Moon, R. Humphry-Baker, J.-H. Yum, J. E. Moser, M. Grätzel, and N.-G. Park, "Lead Iodide Perovskite Sensitized All-Solid-State Submicron Thin Film Mesoscopic Solar Cell with Efficiency Exceeding 9%," Sci. Rep., vol. 2, Aug. 2012.

[13] Y. Ma, S. Wang, L. Zheng, Z. Lu, D. Zhang, Z. Bian, C. Huang, and L. Xiao, "Recent Research Developments of Perovskite Solar Cells," Chin. J. Chem., vol. 32, no. 10, pp. 957–963, Oct. 2014.

[14] J. Burschka, N. Pellet, S.-J. Moon, R. Humphry-Baker, P. Gao, M. K. Nazeeruddin, and M. Grätzel, "Sequential deposition as a route to high-performance perovskite-sensitized solar cells," Nature, vol. 499, no. 7458, pp. 316–319, Jul. 2013.

[15] J. Liu, Y. Wu, C. Qin, X. Yang, T. Yasuda, A. Islam, K. Zhang, W. Peng, W. Chen, and L. Han, "A dopant-free hole-transporting material for efficient and stable perovskite solar cells," Energy Environ. Sci., vol. 7, no. 9, p. 2963, Jun. 2014.

[16] J.-H. Im, I.-H. Jang, N. Pellet, M. Grätzel, and N.-G. Park, "Growth of CH3NH3PbI3 cuboids with controlled size for high-efficiency perovskite solar cells," Nat. Nanotechnol., vol. 9, no. 11, pp. 927–932, Aug. 2014.

[17] H.-S. Kim, J.-W. Lee, N. Yantara, P. P. Boix, S. A. Kulkarni, S. Mhaisalkar, M. Grätzel, and N.-G. Park, "High Efficiency Solid-State Sensitized Solar Cell-Based on Submicrometer Rutile TiO 2 Nanorod and CH 3 NH 3 PbI 3 Perovskite Sensitizer," Nano Lett., vol. 13, no. 6, pp. 2412–2417, Jun. 2013.

[18] Y. Wang, T. Gould, J. F. Dobson, H. Zhang, H. Yang, X. Yao, and H. Zhao, "Density functional theory analysis of structural and electronic properties of orthorhombic perovskite CH 3 NH 3 PbI 3," Phys Chem Chem Phys, vol. 16, no. 4, pp. 1424–1429, 2014.

[19] G. Niu, X. Guo, and L. Wang, "Review of recent progress in chemical stability of perovskite solar cells," J Mater Chem A, vol. 3, no. 17, pp. 8970–8980, 2015.

[20] G. Niu, W. Li, F. Meng, L. Wang, H. Dong, and Y. Qiu, "Study on the stability of CH 3 NH 3 PbI 3 films and the effect of post-modification by aluminum oxide in all-solid-state hybrid solar cells," J Mater Chem A, vol. 2, no. 3, pp. 705–710, 2014.

[21] T. A. Berhe, W.-N. Su, C.-H. Chen, C.-J. Pan, J.-H. Cheng, H.-M. Chen, M.-C. Tsai, L.-Y. Chen, A. A. Dubale, and B.-J. Hwang, "Organometal halide perovskite solar cells: degradation and stability," Energy Env. Sci, vol. 9, no. 2, pp. 323–356, 2016.

[22] R. K. Misra, S. Aharon, B. Li, D. Mogilyansky, I. Visoly-Fisher, L. Etgar, and E. A. Katz, "Temperature- and Component-Dependent Degradation of Perovskite Photovoltaic Materials under Concentrated Sunlight," J. Phys. Chem. Lett., vol. 6, no. 3, pp. 326–330, Feb. 2015.

[23] A. Kojima, K. Teshima, Y. Shirai, and T. Miyasaka, "Organometal Halide Perovskites as Visible-Light Sensitizers for Photovoltaic Cells," J. Am. Chem. Soc., vol. 131, no. 17, pp. 6050–6051, May 2009.

[24] R. Fickler, R. Lapkiewicz, W. N. Plick, M. Krenn, C. Schaeff, S. Ramelow, and A. Zeilinger, "Efficient Hybrid Solar Cells Based on Meso-Superstructured Organometal Halide Perovskites," Science, vol. 338, no. 6107, pp. 640–643, Nov. 2012.

[25] M. Liu, M. B. Johnston, and H. J. Snaith, “Efficient planar heterojunction perovskite solar cells by vapour deposition,” Nature, vol. 501, no. 7467, pp. 395–398, Sep. 2013.

[26] N. Schwartz, P. Temkin, S. Jurado, B. K. Lim, B. D. Heifets, J. S. Polepalli, and R. C. Malenka, “Interface engineering of highly efficient perovskite solar cells,” Science, vol. 345, no. 6196, pp. 535–542, Aug. 2014.

[27] J.-H. Im, J. Luo, M. Franckevičius, N. Pellet, P. Gao, T. Moehl, S. M. Zakeeruddin, M. K. Nazeeruddin, M. Grätzel, and N.-G. Park, “Nanowire Perovskite Solar Cell,” Nano Lett., vol. 15, no. 3, pp. 2120–2126, Mar. 2015.

[28] “Concentrator photovoltaics,” Wikipedia, the free encyclopedia. 20-Mar-2016.

[29] “Finite-difference time-domain method,” Wikipedia, the free encyclopedia. 13-Feb-2016.

[30] “Finite difference method,” Wikipedia, the free encyclopedia. 17-Mar-2016.

[31] “Understanding the FDTD Method.” [Online]. Available: http://www.eecs.wsu.edu/~schneidj/ufdtd/. [Accessed: 20-Mar-2016].

[32] “FDTD Solutions | Lumerical’s Nanophotonic FDTD Simulation Software.” [Online]. Available: https://www.lumerical.com/tcad-products/fdtd/. [Accessed: 20-Mar-2016].

[33] “Finite element method,” Wikipedia, the free encyclopedia. 16-Feb-2016.

[34] “Finite Element Analysis(MCEN 4173/5173) 2006 Fall.” [Online]. Available: http://www.colorado.edu/MCEN/MCEN4173/lecture_notes.html. [Accessed: 20-Mar-2016].

[35] “ANSYS Mechanical Enterprise structural analysis software for FEA | ANSYS.” [Online]. Available: /Products/Structures/ANSYS-Mechanical-Enterprise. [Accessed: 20-Mar-2016].

[36] A. Abate, T. Leijtens, S. Pathak, J. Teuscher, R. Avolio, M. E. Errico, J. Kirkpatrik, J. M. Ball, P. Docampo, I. McPherson, and H. J. Snaith, “Lithium salts as ‘redox active’ p-type dopants for organic semiconductors and their impact in solid-state dye-sensitized solar cells,” Phys. Chem. Chem. Phys., vol. 15, no. 7, p. 2572, 2013.

[37] “Guide to Interpreting I-V Curves.pdf.” .

[38] S. Mathew, A. Yella, P. Gao, R. Humphry-Baker, B. F. E. Curchod, N. Ashari-Astani, I. Tavernelli, U. Rothlisberger, M. K. Nazeeruddin, and M. Grätzel, “Dye-sensitized solar cells with 13% efficiency achieved through the molecular engineering of porphyrin sensitizers,” Nat. Chem., vol. 6, no. 3, pp. 242–247, Feb. 2014.

[39] Y. Han, S. Meyer, Y. Dkhissi, K. Weber, J. M. Pringle, U. Bach, L. Spiccia, and Y.-B. Cheng, “Degradation observations of encapsulated planar CH 3 NH 3 PbI 3 perovskite

solar cells at high temperatures and humidity," J Mater Chem A, vol. 3, no. 15, pp. 8139–8147, 2015.